

Comparison of In-Situ Aerosol Extinction and Scattering Coefficient Measurements Made During the Aerosol Intensive Operating Period

A.W. Strawa¹, R. Elleman², A.G. Hallar³, D. Covert², K. Ricci⁴, R. Provencal⁴, T. W. Owano⁵,
H.H. Jonsson⁶, B. Schmid⁷, A.P. Luu⁸, K. Bokarius⁸, E. Andrews⁹

¹NASA-Ames Research Center, Moffett Field, CA 94035

²University of Washington, Seattle, WA 98195

³NRC, NASA-Ames Research Center, Moffett Field, CA 94035

⁴Picarro, Inc., Sunnyvale, CA 94085 (currently at Los Gatos Research, Inc., Mountain View, CA 94041)

⁵ Los Gatos Research, Inc., Mountain View, CA 94041

⁶CIRPAS/Naval Postgraduate School, Marina, CA 93933

⁷BAER Institute, Sonoma, CA 95476

⁸San Jose State University, San Jose, CA 95192

⁹CIRES, University of Colorado, Boulder, CO 80305

Abstract

In May 2003, the Department of Energy (DOE) Atmospheric Radiation Measurement (ARM) Program sponsored the Aerosol Intensive Operating Period (AIOP) which was conducted over the ARM Climate Research Facility (ACRF) in central Oklahoma. One new instrument that flew in the AIOP, called Cadenza, employed a cavity ring-down technique to measure extinction coefficient and a reciprocal nephelometer technique to simultaneously measure scattering coefficient. This instrument is described in this paper and measurements are compared to those of conventional instrumentation. Agreement between Cadenza extinction coefficient and that derived from combining nephelometer scattering and PSAP absorption (Neph+PSAP) was excellent, about 2%. Agreement between Cadenza scattering coefficient and TSI nephelometer scattering was also excellent, about 2%, well within the uncertainty of the nephelometer and Cadenza scattering measurements. Comparisons between these instruments, made for the special case of plumes, showed that Cadenza measured extinction and scattering several percent higher on average than the Neph+PSAP and nephelometer alone. This difference is likely due to differences in the instrument response time: the response time for Cadenza is 1 sec while that for the nephelometer is a minimum of 8 sec. Plumes, identified as originating from Siberian biomass burning, are characterized. Composite size distributions from wing-mounted probes showed that two of the plumes had significant large particle modes that resulted in high values of the effective radius. The effect of the large particle mode was not seen in the Ångström coefficient calculated from the in-cabin scattering measurements because of the characteristics of the aircraft inlet.

1. Introduction

Past studies have shown that aerosols can have significant effects on the balance of radiation in the atmosphere and may be a threat to human health. These effects can manifest themselves globally as well as locally on climate, the hydrological cycle, and air pollution [Chylek and Coakley, 1974; Dubovik *et al.*, 2000; Horvath, 1993; Ramanathan *et al.*, 2001]. One of the biggest obstacles to a better understanding of these effects and an improved ability to model climate is an inadequate knowledge of the optical properties and spatial distribution of atmospheric aerosols. This deficiency is regarded as one of the primary contributors to uncertainty in climate change predictions [Houghton *et al.*, 2001; Seinfeld, 2004]. Radiative forcing due to aerosols has been identified as one of the most uncertain components of climate change models and as a topic urgently in need of further research [Houghton *et al.*, 2001]. As an example, the global-average direct forcing due to aerosols is estimated to be $-0.4 (\pm 0.3) \text{ Wm}^{-2}$, compared with $2.4 (\pm 0.3) \text{ Wm}^{-2}$ for greenhouse gases [Hansen *et al.*, 1998]. The indirect forcing due to aerosols is estimated to be nearly of equal magnitude to greenhouse gas forcing although of opposite sign. Thus the uncertainty associated with aerosol forcing is not known sufficiently to define the effect of aerosol forcing on future climate change [Houghton *et al.*, 2001].

The effects of aerosol radiative forcing on the regional climate can be much larger than it is on the global climate (i.e., when averaged over the entire planet) [Kiehl and Briegleb, 1993; Russell *et al.*, 2001]. During the Indian Ocean Experiment (INDOEX), Ramanathan *et al.* [2002] found that pollution haze is transported far beyond the source region. These pollutants scatter and absorb incoming solar radiation and thus reduce up to 10% of the solar energy reaching the ocean, and between 10 to 20% over land masses [Ramanathan *et al.*, 2002]. These findings have

raised serious questions related to the impact of atmospheric pollutants on health, marine life, plant ecosystems, and agriculture [*Ramanathan et al.*, 2002], and have underscored the need for improved knowledge of aerosol optical properties. One of the objectives of the DOE ARM program is to improve the treatment of radiative processes in global climate models. In pursuit of this objective, ARM has sponsored the Aerosol Intensive Operating Project (AIOP), which took place at the Southern Great Plains (SGP) ARM Climate Research Facility (ACRF) site in May of 2003. One of the objectives of the AIOP was to test new instrumentation for improved characterization of aerosol optical properties. This paper focuses on a description of one of these instruments, Cadenza, and compares its measurements with those of more standard instruments, and characterizes the aerosol optical properties measured during the AIOP.

Cadenza uses a cavity ringdown (CRD) technique to measure aerosol extinction and a reciprocal nephelometer to measure aerosol scattering. The in-situ measurement of extinction coefficient is difficult because of the wide range of attenuation due to aerosol for different locations and times. In the troposphere, the magnitude of the extinction coefficient can vary from on the order of 1 Mm^{-1} in pristine, uninhabited regions to 1000 Mm^{-1} in polluted regions [*Seinfeld and Pandis*, 1998]. In the stratosphere, background levels of aerosol extinction can be as low as 10^{-2} Mm^{-1} [*Fromm et al.*, 1999]. Currently, in-situ measurement of aerosol extinction requires very long path lengths and is primarily restricted to measurements of surface visibility [*Heintzenberg et al.*, 1997]. The climatic importance of aerosols, however, has resulted in several attempts to measure extinction in-situ on aircraft [*Gerber*, 1979a; *Gerber*, 1979b; *Reid et al.*, 1998; *Weiss and Hobbs*, 1992]. None of these instruments had sufficient sensitivity to measure typical levels of atmospheric aerosol extinction coefficient. CRD is an innovative technique that can achieve high sensitivity by increasing the effective pathlength attainable in a small cell. Cadenza is the first

application of this technique in an instrument designed to operate on aircraft. The AIOP was the first mission where Cadenza extinction and scattering could be compared with other in-situ measurements on an aircraft.

Previous efforts to measure aerosol extinction with CRD are few. Sappey et al [1998] used a pulsed Nd-YAG laser source at 532 and 355 nm wavelength in a one meter cell to measure an extinction coefficient of $2 \times 10^{-7} \text{ m}^{-1}$ (0.2 Mm^{-1}). They compared the sensitivity of their system to that of a Met One Model 237H laser particle counter that uses light scattering to detect individual aerosol particles. *Van der Wal and Ticich* [1999] also used a pulsed system to measure soot volume fraction in flames. They were able to measure an extinction coefficient of 40 Mm^{-1} in a 1 cm sooting flame. More recently, *Smith and Atkinson* [2001] used a pulsed CRD system with a Nd-YAG laser to measure aerosol extinction at wavelengths of 532 and 1064 nm in a one meter cell. This system was similar to that of Sappey et al. and recorded an extinction of about 50 Mm^{-1} at a wavelength of 532 nm. A similar system has been developed at the Desert Research Institute, Reno, NV [*Moosmüller et al.*, 2005] and at the Cooperative Institute for Research in the Environmental Sciences (CIRES), Boulder, CO [*Pettersson et al.*, 2004]. Cadenza was developed in 2002 by Picarro, Inc. under a Small Business Innovative Research project with NASA. A prototype of Cadenza is described in Strawa et al. [2003].

2. Measurements

2.1. DOE Aerosol IOP

In May 2003 DOE conducted the AIOP experiment at the SGP ACRF site in Oklahoma. The objectives of the study were to validate aerosol profiles made by the facility Raman lidar (see

Ferrare et al. [this issue] and Schmid et al. [this issue]), compare new instrumentation designed for the measurement of aerosol optical properties and explore the accuracy with which these properties can be measured. The experiment was conducted during the month of May with the Center for Interdisciplinary Remotely-Piloted Aircraft Studies (CIRPAS) Twin Otter aircraft [Bane et al., 2004; Bluth et al., 1996]. Instrumentation included a TSI (model 3563, TSI St. Paul, MN) nephelometer, an improved version of the 3-wavelength filter-based Particle Soot Absorption Photometer (PSAP) ($\lambda = 467, 530, 660$ nm), similar to the instrument described in Virkkula et al. [2005], three nephelometers (Model RR903, Radiance Research, Seattle, WA) with a humidification system to measure fRH (all operated by the University of Washington), a new photoacoustic instrument on its maiden flight (developed and operated by Desert Research Institute [Arnott et al., this issue], our Cadenza instrument, size distribution instrumentation (Passive Cavity Aerosol Spectrometer Probe (PCASP) and Cloud, Aerosol, and Precipitation Spectrometer (CAPS), operated by CIRPAS), a tandem DMA (operated by Caltech), the Ames Airborne Tracking Sunphotometer 14 channel (AATS-14) [Schmid et al, this issue], and radiometers, some of which were on a stabilized platform (operated by Naval Research Center, Monterey). Sixteen flights were conducted with a focus on flying altitude profiles over the ACRF site. A more complete description of the flights is contained in Schmid, et al. [this issue]. Our objectives during the AIOP were to demonstrate the performance of Cadenza, make comparisons with other in-situ instruments and the remote measurements from the sunphotometer.

2.2. Cavity Ring-Down Applied to Aerosol Optical Property Measurement – CADENZA

2.2.1 Instrument Description

Since the cavity ring-down technique was first demonstrated by O’Keefe and Deacon [1988] it has been used primarily for absorption spectroscopy [O’Keefe *et al.*, 1999]. An excellent review of the CRD techniques and applications can be found in the collection of papers edited by Busch and Busch [1999]. The principle behind CRD is briefly described here using the so-called ‘ping-pong’ model. A pulse of laser light is injected into a cavity that consists of two highly reflective mirrors. The mirror reflectivity is typically better than 99.96%. The laser pulse bounces between the two mirrors inside the ring-down cavity like a ping-pong ball. Each time the pulse interacts with the back mirror, a small amount of light (e.g., 0.04%) leaks out. This light is collected and detected with a photomultiplier or similar detector. The intensity of the light leaking out of the back of the ring-down cavity decreases exponentially when the laser is turned off. It can be shown that the exponential decay, or ring-down time, is related to the mirror reflectivity and the extinction of the material inside the cavity by the relationship

$$\tau = \frac{L}{c} \left((1 - R) + \sigma_{ep} L + \sigma_{sg} L + \sigma_{ag} L \right)^{-1} \quad (1)$$

where L is the cell length, c is the speed of light, R is the mirror reflectivity, σ_{ep} is the coefficient of extinction due to aerosol, σ_{sg} is the coefficient of Rayleigh scattering by gases, and σ_{ag} is the coefficient of absorption due to gaseous species in the cell (Note that extinction is the sum of scattering plus absorption). Laser wavelengths are chosen to minimize absorption by gases.

In the present approach, the extinction coefficient is given by the difference between measurements made when the cell contains a particulate-laden flow and when the particulate is filtered out:

$$\sigma_{ep} = \frac{1}{c} \left(\frac{1}{\tau_{ep}} - \frac{1}{\tau_0} \right) \quad (2)$$

where τ_{ep} is the ring-down time of the aerosol-laden flow and τ_0 is for the filtered air. Thus the effect of mirror reflectivity and Rayleigh scattering or any residual gas absorption is eliminated from the measurement. The minimum detectable extinction of continuous wave cavity ring down (CW-CRD) systems is on the order of 10^{-1} to 10^{-3} Mm^{-1} . [Paldus and Zare, 1999] Thus, a measurement precision of 1% to 0.01% in the extinction coefficient is theoretically achievable at extinction levels of 1 Mm^{-1} .

In this application a continuous wave (CW) laser source is used which results in several advantages over the pulsed laser technique [Romanini et al., 1997]. First, the resulting overlap between the laser and cell linewidth results in actual energy build up in the cell. It is this build up of energy that allows for the simultaneous measurement of scattering and extinction in the same cell. In Cadenza, once the laser wavelength is in resonance with the cavity, the laser is turned off rapidly (tens of nsec), and the resultant ring-down is recorded. The use of CW lasers allows for a sample rate of up to 4000 per second which is faster than pulsed lasers can achieve. Finally, the use of CW laser diodes allows for a more compact and rugged instrument suitable for aircraft operations. Pulsed laser systems are larger and their sample rate is limited by the repetition rate of the laser, typically about 100 Hz.

Cadenza is a Cavity Ring-Down Spectroscopy (CRDS) system designed to measure aerosol extinction and scattering simultaneously. The prototype instrument is described in Strawa et al. [2003]. Figure 1 shows a schematic of the instrument in its current configuration. The optical cavity is composed of four highly reflective, dual-coated mirrors in a folded configuration called a ‘bow-tie’ configuration. In this configuration, an 81.8 cm pathlength is folded into a 15 cm x

20 cm cell. The cell is 2 cm high. The effective pathlength, which is determined primarily by the mirror reflectivity, is approximately 2 km. The mirrors are coated to reflect laser light at 675 nm and 1550 nm. The mirror pairs are mounted 20 cm apart with 6 cm separating the mirrors on each side. The lasers are located in the lower right quadrant of the optical bench. Visible light at 675 nm was generated by a CW laser diode (Power Technologies Inc., Model SAPM 2016079) and near infrared light at 1550 nm was generated by a distributed feedback laser (NTT Electronics Model 015506). The light is conditioned with lenses, pinholes, and optical isolators. Standard mirrors are used to direct the beam into the cell. Ring-down signals are detected at the opposite end of the cell (top of figure) by two photodetectors. Advantages of the ‘bow-tie’ configuration are a long pathlength in a small space and ease of alignment. Mirror reflectivity, R , is 0.999923 and 0.999958 at 675 nm and 1550 nm respectively. The cavity is characterized by its free spectral range and finesse. The free spectral range is the spacing in frequency between two adjacent peaks in the cavity transmission curve and is calculated as the ratio of the speed of light and the path length [Siegman, 1986]. For our bow-tie system, the unfolded pathlength is 81.8 cm which gives a free spectral range of about 375 MHz. Finesse is the resolution of the cavity and is equal to $\pi R^{0.25} / (1 - R^2)$ for a four mirror cavity [Siegman, 1986]. Cadenza’s cavity has a finesse of 20400 and 38000 in the visible and near IR respectively.

Air enters the cell at the sample inlet, turns 90 deg in a small plenum, and is then expanded to fill the cross-section of the test cell, which is 10 mm by 15 cm. The aerosol flowrate through the instrument is 3 L min^{-1} and a 90 deg bend in a tube with 0.008 m inner diameter will pass 96% of $8 \mu\text{m}$ diameter particles. The sample flow direction is transverse to the optical path, resulting in a very fast response time. Clean purge flow enters the cell via two inlets that are located between the aerosol flow and the mirrors. The purpose of the purge flows is to keep the highly-reflective

mirrors clean from aerosol particles and semi-volatile gases. The purge flow consists of sample air that has been filtered with a low pressure drop filter (Pall). The purge flows are momentum matched to the sample flow providing a laminar slipstream. Smoke visualization studies confirm that the 15 cm sample length is maintained over a relatively wide range of flow conditions (See Figure 2). The cell ring-down mirrors are heated to 40C to prevent condensation; however the mirrors and their mounts are thermally isolated from the rest of the flow cell, keeping the sample flow as close to ambient conditions as possible.

One advantage of the CW-CRD system is its small size and insensitivity to vibration. The optical head is 18 inches wide x 22 deep x 8 high, easily fitting into a standard 19 inch equipment rack. Figure 3 is a picture of the instrument. While some effort was made to package the electronics, computer, and pump equipment into rack-mountable boxes, a dramatic reduction in instrument size and weight is easily possible.

As mentioned, with CW-CRD, the laser is in resonance with the ring-down cell allowing laser power build up in the cell [*Romanini et al.*, 1997]. For a cell with non-absorbing mirrors and negligible internal losses, the peak circulating intensity is approximately given by

$$I_{circ} \approx I_{inc} / T \quad (3)$$

where I_{inc} is the incident intensity and T is the mirror transmittance [*Siegman*, 1986]. This build up of energy within the cell makes it possible to detect the light scattered by the aerosol. For our system, $I_{inc}=20$ mW, and $T = 0.0004$. Equation 3 then gives a maximum theoretical circulating power of about 50 W. This estimate does not account for other losses within the cell. Additionally, the laser is switched off well before this maximum is achieved to allow the cell to ring-down. Operationally, an energy density of about 2 W cm^{-2} within the cell is typical. Energy

densities are not high enough to affect sample conditions. To illustrate, the radiant heat to a particle can be described as

$$\alpha QA = c_p m dT/dt \quad (4)$$

where Q is the heat flux estimated to be 2 W cm^{-2} , α is the absorptivity of the particle (the amount of radiant energy actually transferred to the particle by absorption), A is the cross-sectional area of a particle (assumed to be $0.15 \text{ }\mu\text{m}$ in radius), c_p is the specific heat of water ($1952 \text{ J kg}^{-1} \text{ K}^{-1}$), m is the mass of the particle (assuming a density of 1 g m^{-3}), dT is the temperature difference from ambient temperature in degrees K, and dt is the length of time the particle undergoes heating. A highly absorbing atmospheric aerosol can have an absorptivity of as high as 0.3. The heat load experienced by the particle will be the exponentially decreasing laser power integrated over the $8 \text{ }\mu\text{s}$ ringdown time. For this calculation we will assume a constant maximum heating for $3 \text{ }\mu\text{s}$. This yields a dT of 0.18 K . Wexler and Seinfeld [1990] have estimated the timescale for a solid particle to come into equilibrium with its environment to be several minutes. Further, the timescale increases with increasing particle water content [Seinfeld and Pandis, 1998]. Assuming a sample flowrate of 3 L min^{-1} and a beam waist of 3 mm , the particle will spend 0.24 sec in the beam. Therefore, whatever small change the particle will undergo due to the slight temperature increase imposed by the laser will not be seen in the measurement volume.

The scattering signal is collected with two diffusers set into the cell wall above the point where the optical beams cross. The diffusers (Gamma Scientific Model 700-8D) have a Lambertian response from 5 to 175 deg . The diffuser for the 675 nm channel is connected to a photomultiplier tube (Hamamatsu Model R1464) with a light pipe. The diffuser for the 1550 nm channel is connected to an avalanche photodiode with a fiber optic cable. In a typical

nephelometer design, the light source is transmitted through a diffuser or lens and the detector senses along an optical path (see e.g. [Anderson *et al.*, 1996]). In our system, the optical arrangement is a modification of the ‘reciprocal’ nephelometer design of Mulholland and Bryner [1994], wherein the illumination is provided by a laser along an optical path and the detector is mounted orthogonally to the optical and flow axes to collect the light. There are several advantages to this approach. First, it is possible to obtain better Lambertian diffusers for detection than is commonly used to disperse light sources. Since we use a laser source, corrections for the spectral characteristics of the detector and filter assembly or of the light source are not required. One disadvantage to this system is that the laser light is polarized, typically perpendicular to the plane defined by the optics, and must be accounted for. We have attempted to mitigate this fact by placing the detector and diffuser at approximately 45 degrees to the optical plane where the effect of polarization is negligible.

A system of automated valves is located at the inlet to the flow cell. This allows us to alternate between aerosol-laden and filtered air in an implementation of Equation 2. For flight applications, a ‘zero’ or filtered measurement is made for one minute out of every 6 minutes and the zero-air ringdown time before and after a measurement period was averaged before calculating this extinction coefficient using Equation 2. The cell is extremely stable, and the largest factor affecting the zero-air ringdown is the change in Rayleigh scattering due to changes in pressure as the aircraft changes altitude. By monitoring the zero-air ring-downs we are able to correct for changes in Rayleigh scattering directly without having to assume that the Rayleigh scattering is a function of pressure. For ground applications, the zero ring-down need not be taken as often.

Typical ring-down times for the instrument are 8.2 μs for the 675 nm channel and 16.2 μs for the 1550 nm channel and can be measured to an accuracy of approximately 1% per shot. There are 100 shots to a 1 sec sample measurement. This difference between the visible and infrared ring-down times of a factor of two is reflective of the fact that the 1550 nm laser is better matched to the ring-down cell and that the mirrors are more reflective at this wavelength.

The ring-down signal is an exponential decay that is sampled at 10 MHz by a Gage Compuscope 12100 data acquisition card. The exponential decay is fit with a Levenberg-Marquardt (L-M) algorithm [Press *et al.*, 1986] to obtain the ring-down time, τ , and the intensity. Each channel runs independently at about 100 Hz. After one second, the individual τ 's are averaged to produce a measurement.

The scattering signal also decays exponentially as the laser intensity decreases in the ring-down cell. The scattering signal is fit to an exponential decay as is the ring-down signal using an L-M algorithm. The scattering signal must be referenced to the incident laser intensity just as in standard nephelometry. Strawa et al. (2003) showed that the ring-down intensity is related to the incident intensity. In practice, Equation 4 in Strawa et al. (2003) becomes:

$$\sigma_{sp} = \left(\frac{I_{sp}}{I_{rd}} \right) \frac{(1-R)}{(1+R)L} K_S \quad (5)$$

where σ_{sp} is the scattering coefficient, I_{sp} is the scattered light intensity, I_{rd} is the intensity of light measured at the ring-down detector, R is the mirror reflectivity, L is the cell length, and K_S is the scattering calibration constant, that is a function of particle size.

2.2.2. Cadenza Calibration

Performance of Cadenza was tested at the Aerosol Lab at NASA-Ames Research Center. An aerosol stream of polystyrene latex (PSL) calibration spheres (Duke Scientific) was produced by atomizing a water solution of the spheres and passing the resulting polydisperse aerosol through a TSI Model 3081 electrostatic classifier. This produced a stream of monodisperse aerosol that was sampled by Cadenza and a TSI 3025 condensation particle counter (CPC). Particle diameters of 500, 700, and 900 nm are used in calibration. Particle concentration was varied to produce aerosol extinction coefficients from 1 to 200 Mm^{-1} . Since the number density of the aerosol is known from the CPC and the diameter of the particles is controlled by the electrostatic classifier, the theoretical Mie extinction can be calculated using the refractive index of 1.52 at 675 nm provided by the manufacturer. This theoretical result is compared to the extinction and scattering measurements made by Cadenza. Since the calibration spheres are non-absorbing, the scattering and extinction coefficients are equal. The multi-wavelength measurement allows us to use the Ångström coefficient, based on the two Cadenza extinction channels to correct for truncation errors in the scattering measurement.

Examples of calibration plots for our three channels of 675 nm extinction, 675 nm scattering, and 1550 nm extinction are shown in Figure 4 a, b, and c, respectively. Three calibration runs, one for each of 500 nm, 700 nm, and 900 nm diameter PSL are combined on each plot. Extinction and scattering (these are the same for PSL) are calculated from the measured CPC number density and PSL size distributions provided by the manufacturer. Scanning mobility particle sizing (SMPS, TSI model 8081) size distributions of each size PSL were obtained using a second, identical, SMPS system, but these distribution did not have adequate size resolution for calibration purposes. The calculated parameters are plotted against the Cadenza measured values in scatter plots. The excellent instrument linearity, repeatability, and accuracy are evident in the

plots. The uncertainty for typical extinction levels is governed by two factors: instrument performance and variations caused by the number of particles in the sample volume as discussed in Pettersson et al. [2004]. Based on our calibrations and our ability to measure filtered air flows we have determined instrument accuracy to be 2% of 1 Mm^{-1} 675 nm extinction levels averaged over 8 sec, 10% of 1 Mm^{-1} 675 nm scattering levels averaged over 8 sec, and 2% for 5 Mm^{-1} 1550 nm extinction averaged over 8 sec. The minimum detection limit for a CRD aerosol instrument is dominated by the statistics of low number concentrations of particles in the sample volume [Pettersson et al., 2004] and is a function of the size of particles being measured. Cadenza sample volume is approximately 2 cm^3 . We estimate our sensitivity in extinction to be about 0.3 Mm^{-1} in the visible and 0.5 Mm^{-1} in the infrared for an 8 sec average. An 8 sec averaging time is used here for comparison with the nephelometer data presented later in the manuscript. We could not obtain a measurable 1550 nm scattering signal during calibration. While we did obtain measurable 1550 nm scattering signals during the AIOP, these are not reported because they are not calibrated. We are working on the ability to generate a larger number of large, supermicron particles in our laboratory so that the 1550 nm scattering channel can be calibrated.

2.3 Conventional Scattering and Absorption Measurements

During the AIOP, Cadenza measurements of aerosol scattering were compared to conventional measurements of scattering from a TSI Model 3536 nephelometer and Cadenza extinction was compared to the sum of scattering from a nephelometer and absorption from a 3-wavelength PSAP that was operated by the University of Washington. Light-scattering data were obtained from a TSI Model 3563 integrating nephelometer (St. Paul, MN) at 450, 550, 700 nm

wavelengths. The nephelometer was calibrated against particle-free air and CO₂ during the field deployment and was zeroed with particle-free air before each flight. Scattering coefficient data were corrected using the procedures outlined in Anderson et al. [1996] and Anderson and Ogren [1998]. The nephelometer $\sigma_{sp}(\lambda)$ values were adjusted and reported from their blue, green and red center wavelengths (450, 550, 700 nm) to those of the PSAP instrument (467, 530, 660 nm) using the Ångström relationship derived from the nephelometer.

Aerosol light absorption $\sigma_{ap}(\lambda)$ was measured using an improved version of the 3-wavelength PSAP ($\lambda = 467, 530, 660$ nm), that was similar to the instrument described in *Virkkula et al.* [2005]. In the PSAP, a light source illuminates a sample and a reference filter. Detectors are placed behind the filters. Aerosol-laden flow is collected on the sample filter and the attenuation of light through that filter is measured by the detector. A simple calculation for determining the absorption coefficient from a filter-based measurement is given by

$$\sigma_{ap} = \frac{A}{V} \ln \left[\frac{I_0}{I} \right] \quad (6)$$

where A is the area of the sample spot, V is the volume of air drawn through the filter and I_0 and I are the reference and sample average filter transmittances during the measurement. The sample intensity varies with time; a continuous measurement of the absorption coefficient can be obtained within the precision of the sample detector. The advantages of this class of instruments are that they are easy to use, relatively inexpensive, and suitable for unattended operation; however, Equation 6 cannot be used to give the absorption coefficient directly because several corrections need to be made. Both the scattering and absorption of the particles collected on the filter will affect the apparent absorption measured by the instrument [*Bond et al.*, 1999; *Clarke et al.*, 1987; *Horvath*, 1997] and corrections for these effects are complex [*Bond et al.*, 1999;

Virkkula et al., 2005]. The instrument is also sensitive to changes in relative humidity [*Arnott et al.*, 2003]. The data reduction and correction scheme of *Bond et al.* [1999] was applied to the absorption data. The PSAP measured downstream of the TSI nephelometer, typically at the conditions of the nephelometer, i.e., dry and at an elevated temperature. In this analysis, absorption coefficient was not corrected to the higher relative humidity (RH) of the ambient air.

The hygroscopic behavior of the aerosol was determined from the three Radiance Research (RR) single wavelength (550 nm) nephelometers (Model RR903, Radiance Research, Seattle, WA) [*Gassó et al.*, 2000]. Dried aerosol from the TSI nephelometer was fed into the humidification system a flow rate of 6 L min⁻¹. The three RR nephelometers were operated at three different RH settings: below ambient, near 85%, and at an intermediate RH level.

2.4. Sampling Considerations

Aerosol was sampled from a shrouded inlet. This inlet is described and characterized in Hegg et al. [accepted] as having no appreciable loss in transmission efficiency for particles with diameters below 3.5 μm. The efficiency thereafter decreases rapidly but levels off at an efficiency of slightly better than 0.6 for particles 5.5 μm in diameter through the limit of their measurements at 9 μm.

The TSI nephelometer was operated at a flow rate of 30 L min⁻¹ and with its inlet heater operational at near 35°C. This results in considerably lower RH inside the instrument than the ambient RH. The RH inside the TSI nephelometer ranged from near 0 to 35% depending on ambient RH. While not deliberately heated, the sample air inside Cadenza was nearly at the temperature of the aircraft cabin and consequently drier than the ambient air. This was caused

partially by ram heating at the aerosol inlet and partially due to heating of the sample line as it carried aerosol from the inlet to the instrument.

In this paper, all in-situ measurements have been corrected for the effective scattering increase due to particle growth in the presence of humidity, parameterized by [Kasten, 1969]

$$\sigma_{sp}(RH) = \sigma_{sp}(RH_0) \left(\frac{100 - RH}{100 - RH_0} \right)^{-\gamma} \quad (7)$$

In Equation 7, $\sigma_{sp}(RH)$ is the scattering coefficient as a function of measured RH , RH_0 refers to a dry, reference RH , and γ is the exponential dependence of light scattering on RH . The dependence of light-scattering on RH was parameterized by the exponent of Equation 7, based on the work of Kasten [1969] (see also Gassó *et al.*, [2000]). The in-situ extinction measurements have also been corrected to ambient temperature and pressure. In the case of Cadenza extinction, the scattering part of the measurement, determined by the Cadenza scattering measurement, is corrected for RH , and the absorbing part, the difference between the extinction and scattering, was not corrected. Redemann *et al.* [2001] have estimated errors of as high as 0.03 in single-scattering albedo, ω , due to the assumption that RH has no affect on absorption. Since no measurements of the effect of relative humidity on the absorption coefficient were made on the aircraft, we did not correct for this effect. The RH correction was determined at a wavelength of 550 nm. Although there is some dependence of fRH on wavelength, this was not considered since no measurement of this wavelength dependence was obtained on the aircraft during the experiment.

Measurements were corrected to a common wavelength (675 nm) using the Ångström relationship with an exponent determined from the three-wavelength TSI nephelometer measurements.

2.5. Considerations of Measurement Uncertainty for Aerosol Optical Properties

Uncertainties in the extinction coefficient measurement of Cadenza will be introduced into the measurement by photon shot noise, digitization noise, particle losses and relative humidity changes within the instrument, and pathlength [Strawa *et al.*, 2003]. Based on our laboratory calibrations, described in Section 2.2.2 and data analysis from these field missions, Cadenza was able to measure an extinction coefficient of 1 Mm^{-1} with an uncertainty of 2% at 675 nm wavelength averaged over 8 sec; an extinction coefficient of 5 Mm^{-1} with an uncertainty of 2% at 1550 nm wavelength averaged over 8 sec; and a scattering coefficient of 1 Mm^{-1} at 675 nm wavelength with an uncertainty of 10 % averaged over 8 sec.

The uncertainty in the scattering coefficient measurement of Cadenza is similar to the uncertainty recorded for TSI Model 3563 nephelometers for particles less than $1 \mu\text{m}$ in diameter [Anderson *et al.*, 1996; Anderson and Ogren, 1998]. The source of this absolute uncertainty is derived from an inability to measure the entire forward scattering lobe of an aerosol sample [Anderson and Ogren, 1998], a problem that our reciprocal nephelometer design shares with the TSI nephelometer. The scattering measurement will also be affected by non-idealities in the angular sensitivity of the instrument. These sources of error are very similar to those experienced by integrating nephelometers. Anderson *et al.* [1996] quote an uncertainty of 9.8% at a wavelength of 700 nm in measurements of scattering coefficient made with the TSI Model 3563 integrating nephelometer based on laboratory closure experiments with non-absorbing aerosols in the accumulation mode (0.1 to $1 \mu\text{m}$ in diameter). They state that this uncertainty is dominated by systematic uncertainties in non-idealities in wavelength and angular response, which are both a function of particle size.

One of the physical limitations of nephelometry is that any real diffuser cannot have a perfectly Lambertian profile (that is perfectly proportional to the cosine of the scattering angle), nor can any instrument measure all scattering angles from 0° to 180° . The intensity of light scattered from a particle is a function of the angle, θ , between the incident beam and the scattered light, the wavelength of the incident light, and particle size, shape and composition. Larger particles scatter more light in the forward direction, near 0° . The combination of limited angular measurement and non-Lambertian light source represent an uncertainty that can only be partially corrected for by truncation error corrections [*Anderson et al.*, 1996; *Anderson and Ogren*, 1998]. Additionally, uncertainties due to the dependence of the scattering on the wavelength of light will depend on the effective linewidth of the instrument. The CRD technique uses a laser of very narrow linewidth and this uncertainty is negligible in Cadenza. Nephelometers are calibrated with gases of known scattering coefficient. One advantage of our instrument is that we can also compare our measurements of extinction and scattering coefficients with lab-generated, non-absorbing spheres to calibrate out effects due to angular non-idealities in the scattering measurement. Making the scattering and extinction measurements simultaneously will eliminate differences in the effects of particle loss and relative humidity changes within the instrument.

2.6. Size Distribution Measurements

Aerosol size distributions were measured with a wing mounted Particle Measuring Systems (PMS) PCASP for $0.11 < D_p < 3.0 \mu\text{m}$ and a wing mounted Droplet Measurement Technology (DMT) CAPS [*Baumgardner et al.*, 2001] probe that was configured to measure particles in the size range of $0.67 < D_p < 63.3 \mu\text{m}$. There are several issues that must be considered before comparing or combining these size distributions. The first issue is measurement conditions. The

PCASP cavity was heated to an elevated but unmeasured temperature resulting in what is generally considered a dry size distribution. The CAPS probe measures size distributions at ambient conditions (RH, P, and T). The second issue is measurement geometry. The PCASP measures over a wide angular range at a scattering angle of near 90° , while the CAPS measures at narrow forward and back scattering angles in the size range $\sim 0.7 < D_p < 50 \mu\text{m}$ and uses an occultation sensor for drops in the range $25 < D_p < 63.3 \mu\text{m}$. Very few particles were observed with diameters greater than $25 \mu\text{m}$ since we were not flying in clouds. Scattering intensities calculated from Mie theory tend to oscillate dramatically between $1 < D_p < 10 \mu\text{m}$, the region of instrument overlap, for these measurement wavelengths and the PCASP geometry is less sensitive to these oscillations than the CAPS geometry. The final issue for consideration is calibration methods. Both instruments are calibrated with polystyrene latex spheres (refractive index of 1.59 at 589 nm) and glass beads (refractive index of 1.56 at 589 nm). Differences between the calibration refractive index and that of the actual aerosol sampled will introduce uncertainties in the size distribution measurements. The departure of the actual particle shape from spherical will introduce additional uncertainties. Uncertainty in particle concentration measured by the probes is dominated by uncertainties in the measurement of the laser active area, which along with the aircraft true airspeed determines the probe's viewing volume. Uncertainty in the PCASP number size distributions is estimated to be 20%, and for CAPS it is estimated to be 30% except in the $1 < D_p < 10 \mu\text{m}$ region, where uncertainties can be as high as a factor of 2 (personal communication with instrument PI, H. Jonsson). Because of the sampling geometry issue, the PCASP is generally regarded as the more accurate instrument in the $0.79 < D_p < 3.0 \mu\text{m}$ overlap region. Considering all of these effects the PCASP measurements were used instead of the CAPS measurements in the overlap region for calculation of effective radius. A

correction for the effect of RH on the PCASP measurements was applied in the calculation of effective radius, as discussed in Section 3.4. The effective radius, r_{eff} , represents the dependence of scattering on particle size and is traditionally defined as [Hansen and Travis, 1974; Mitchell, 2002]

$$r_{eff} = \frac{\int n(r)r^3 dr}{\int n(r)r^2 dr} \quad (8)$$

where r is the geometrical mean radius of the size bin and $n(r)$ is the particle concentration per size bin. We estimate the uncertainty in retrieved effective radius to be 20%.

3. Results

3.1. Comparison of Extinction and Scattering Coefficients

Since Cadenza is a relatively new instrument, it is important to make comparisons between its measurements and those of more standard in-situ measurements of aerosol optical properties. The comparisons in this paper are made at ambient temperature and pressure at 675 nm wavelength. As mentioned, Cadenza and nephelometer scattering and the scattering portion of Cadenza extinction are corrected to ambient relative humidity using Equation 7 with γ determined by the humidification system that included three Radiance Research nephelometers. During AIOP, γ was 0.32 on average with a standard deviation of 0.11. The TSI nephelometer scattering coefficient is adjusted from its reported value of 660 nm to 675 nm using the nephelometer derived Ångström exponent (530nm to 660 nm). The PSAP absorption coefficient was measured at 660 nm and is adjusted to 675 nm assuming a λ^{-1} dependence and no relative humidity correction is made. Cadenza scattering was compared with TSI nephelometer scattering

(Figure 5a) and Cadenza extinction (Figure 5b) was compared with the extinction formed by the sum of nephelometer scattering and PSAP absorption (Neph+PSAP). The plots compare all 8-sec averaged measurements from every flight during AIOP, over 20,700 measurements. The slope of the Cadenza:Neph+PSAP line for extinction is 1.02 and of the Cadenza:Neph line for scattering is 0.98 as shown on the graphs and in Table 1. This agreement is excellent and well within instrument uncertainties.

During the first part of the AIOP mission, the Cadenza scattering signal experienced high noise. The source of this noise was predominantly electronic, originating from one of the instrument circuits. It proved impossible to fully correct for this problem in the field. The electronic noise was effectively decreased, however, during the last several flights by the use of a Stanford Research Systems model SR560 preamp and the scattering signal-to-noise was much improved for these flights. An improved data processing algorithm was also used during these flights. Table 1 shows the slope and correlation coefficient for Cadenza extinction and scattering compared to Neph+PSAP extinction and nephelometer scattering for the last three flights as 1.00 and 0.99 respectively. We see that the slope and correlation does not change appreciably from all flights to the last three for the extinction comparison. The fact that the values for scattering coefficient do not change appreciably from all flights to the last three flights suggests that the 8-sec averaging effectively damps out the noise.

We expected to see more differences between Cadenza and the TSI nephelometer scattering for this experiment for three primary reasons. First, Cadenza does not intentionally heat the sample and should more closely measure at ambient conditions. Second, Cadenza has a more Lambertian diffuser response than the nephelometer light source. This effect would be especially important for the large particles seen in plumes in this experiment. Finally, no wavelength

correction is required with the reciprocal nephelometer concept. Agreement between the two instruments was better than expected for several reasons. The truncation error corrections [Anderson and Ogren, 1999] applied to the TSI measurements worked well, and the University of Washington investigators took care to characterize the filter wavelengths corrections needed for the three channels. Both measurements were made at essentially the same elevated temperature and lower relative humidity, relative to ambient due the heating of the flow in the aircraft cabin. Lower relative humidity would drive off some of the water associated with the hygroscopic particles reducing their size and mitigating the effect of truncation errors.

Figure 5 shows that the overall comparison between Cadenza, the nephelometer, and the PSAP was excellent; however, there is not perfect correlation between the measurements. As an example, on May 7, 2003, the Twin-Otter pilots noted a smoke plume from a grass fire and flew two low-level passes through the plume. Figure 6 shows measurements made during that day's flight. Figure 6a is the altitude profile flown by the Twin-Otter, and Figures 6b and 6c compare Cadenza and Neph+PSAP extinction and Cadenza and Neph scattering respectively for the entire flight. The three plume crossings are identified by circles in Figure 6c and expanded in Figure 6d. The data in Figures 6b and 6c are 8-sec average data, while the data presented in Figure 6d are the original, 1-sec data from the instruments uncorrected for truncation error. The one second data show more clearly the effects of instrument response (The peak magnitude of the 1-sec data is much higher than the 8-sec data due to averaging). The longer response of the nephelometer is due to the fact that its aerosol flow path is aligned with its optical axis and that the sample volume is large, approximately a 1 meter path length. On the other hand, the fast response of Cadenza is due to the fact that the aerosol flow is perpendicular to the optical path and the sample volume is much smaller, with a 20 cm by 5 cm cross section.

Comparisons of Cadenza with nephelometer scattering and Cadenza with nephelometer plus PSAP extinction made for the entire AIOP mission are very good, within 2 %. The agreement between these instruments is not always this good for individual events, especially transient events, as illustrated in Figure 7 which compares measurements made during the flight conducted on May 27. Figure 7a compares Cadenza 675 nm extinction coefficient with nephelometer scattering plus PSAP absorption coefficients corrected to 675 nm. Figure 7b shows a comparison between Cadenza 675 nm scattering coefficient and that of the TSI nephelometer, also corrected to 675 nm. These plots show generally excellent agreement; however, it appears that the nephelometer scattering coefficient is higher than Cadenza during the plumes at 147.727 and 147.752 fractional Julian days by approximately 5 % and 10 % respectively. Cadenza extinction and scattering are independent, simultaneous measurements, with independent uncertainties. On the other hand, while the magnitude of the Neph+PSAP extinction is dominated by nephelometer scattering, its uncertainty is usually dominated by PSAP uncertainty. The events in Figures 7a and 7b show that the difference between the measurements of extinction cannot always be attributed to PSAP uncertainty. In these cases the difference in extinction is due to differences in the scattering measurement.

Figure 7c shows Cadenza extinction measured at 1550 nm wavelength. These data are also averaged over 8-secs and corrected for temperature, pressure and RH using the same method as the 675 nm channel. As discussed in Schmid et al. [this issue] Cadenza 1550 nm extinction differs from that retrieved from the AATS-14 by about 20%. Some of this difference can be attributed to an inadequate fRH correction. For 1550 nm measurements, the effect of wavelength on the fRH correction determined at 550 nm may be significant; however, no information is known about the wavelength dependence on fRH for the aerosol in the airborne portion of this

experiment. Figure 7d shows the altitude profile flown by the Twin-Otter and the ambient relative humidity along the flight path. There may also be some effect of the aircraft inlet characteristics as discussed in section 3.4.

There does not seem to be any significant correlation between the difference of Cadenza and nephelometer measurements with pressure or relative humidity or effective diameter. Nor was there a correlation of instrument measurement difference with the magnitude of the measurement signal for the overall mission, that is to say that one instrument did not measure high for large values of extinction and scattering. However, Cadenza measured larger values in the plume cases as will be discussed in section 3.4.

3.3 Comparison of aerosol Optical Properties in Profiles

Figure 8 shows a comparison between the in-situ 675 nm extinction measured by the Cadenza cavity ringdown instrument, and a vertical extinction profile for 675 nm derived from the AATS-14 sun photometer [Schmid et al., this issue]. AATS-14 measures the optical depth above the aircraft in the absence of clouds at 14 wavelengths and can determine the optical depth due to aerosols and selected gases. Both of these measurement techniques have advantages and disadvantages. Cadenza extinction coefficient must be corrected for the effects of the aircraft inlet; however, it has a very fast time response, and is a direct measure of the extinction. While Cadenza does not alter the temperature and pressure of the aerosol entering its cell, corrections are necessary for changes to the temperature, pressure, and relative humidity that occur in the aircraft sampling inlet. AATS-14 measures at ambient conditions and must be corrected for Rayleigh scattering, gaseous absorption, and diffuse light. The resultant extinction is obtained by differentiating the aerosol optical depth over the altitude profile flown by the aircraft which can

cause some smoothing, as is evident in Figure 8. The most important issue with the sunphotometer derived extinction is the spatial and temporal variability of the aerosol above the aircraft. These issues are thoroughly discussed in Schmid et al. [this issue]. The agreement between the instruments in Figure 8 is remarkable considering that AATS-14 measures the extinction in a line-of-sight trajectory to the sun, while Cadenza measures the local extinction at each point along the aircraft flight path.

Figure 9 shows the vertical extinction profile for four of the profiles flown during the AIOP. Because one of the primary AIOP objectives was to assess the performance of the Raman lidar (see for example Ferrare et al. [this issue] and Schmid et al.[this issue]), a significant portion of flight hours was devoted to profile flight legs. Some profiles were spirals, flown over the ACRF site with a climb rate of 500 ft/min. This rate-of-climb minimized induced changes and lags in the instruments. Other profiles were short duration (5 to 10 min) level legs flown in a stepwise fashion. A list of the profiles considered in this study is shown in Table 2. The large extinction coefficient values measured on May 17 (profile 10) are seen to occur in the boundary layer. Profile 24, which was obtained on May 28, shows a profile typical of most aerosol profiles made during the mission, with extinction values of 20 to 30 Mm^{-1} in the boundary layer, decreasing slightly with altitude. Profiles 22 and 23 were obtained on May 27 when the influence of high altitude aged smoke was prevalent. Slopes, intercepts, and correlation coefficients obtained from scatter plots comparing the extinction and scattering coefficients measured by Cadenza and the nephelometer and PSAP during these profiles are shown in Table 1. The slopes were 0.99 for extinction and 0.96 for scattering, very similar to those made up from data taken during the entire mission.

3.4 Comparison of Aerosol Optical Properties in Plumes

Several plumes were sampled during the AIOP. For purposes of this comparison, a plume is designated as anytime the extinction was above 50 Mm^{-1} for a short period as opposed to extended periods of elevated extinction due to flights in the boundary layer. A list of the 18 identified plumes is shown in Table 3. Most of the low altitude plumes were observed in early May and the plumes above 2.5 km were observed later in the month. The bisector slope, y-intercept, and correlation coefficient obtained from scatter plots comparing extinction and scattering for the instruments for the plume cases are tabulated in Table 1. The plume cases show that the Cadenza extinction (slope = 1.097) and scattering (slope = 1.082) are several percent higher than that from Neph+PSAP and Neph. The y-intercept for the plume cases occurs at -6 Mm^{-1} for extinction and -5 Mm^{-1} for scattering. This is likely due to differences in the time that the nephelometer and Cadenza respond to transients in the aerosol sample. The sampling interval for the nephelometer is approximately 8 sec. based on the nephelometer volume and flowrate (private communication with instrument co-I, R. Elleman). Cadenza can respond faster because the sample flow is perpendicular to the optical axis and the sample length is about $2 \times 10^{-3} \text{ m}$ in the direction of the flow vector. This difference in response time and measurement magnitude is illustrated in Figure 6d. Since there was no indication of a systematic bias between the instruments for the overall mission or in the profiles, we suspect that this difference is due to the different sample flushing times (temporal response) of the instruments that was not fully compensated for when the data were averaged over 8 sec.

Cadenza and Neph+PSAP derived extinction and ω for the plumes listed in Table 3 are plotted in Figure 10a and 10b. The visible low altitude smoke plume, observed on May 7, plumes 0, 1, and 2, have surprising low extinction values, 60 to 70 Mm^{-1} , due to the short duration of the episodes.

Maximum 1-sec extinction levels for these plumes exceeded 400 Mm^{-1} (see Figure 6d), but the extinction levels decreased when averaged over 8-sec. Values of ω for plumes 0, 1, and 2 were not as low as expected for a grass fire smoke plume. Cadenza measured an average ω of 0.918 at 675 nm for the three plumes, while the neph+PSAP average value was 0.941, corrected to 675 nm. These values were considerably higher than values of about 0.85 (at 550 nm) for local smoke plumes previously observed at the SGP site [Sheridan *et al.*, 2001]. Reid and Hobbs [1998] observed ω from 0.75 to 0.85 (at 550 nm) from in-situ measurements of smoke from fresh biomass fires in Brazil. Eck *et al.* [2003] retrieved similar ω values from AERONET measurements in Africa. One possible explanation for this difference is that the optical properties of the Oklahoma plumes were mixed with that of the surrounding air during the 8-sec averaging time of the samples. Values of the average γ for each plume are tabulated in Table 3.

Effective radii, r_{eff} , determined from combined CAPS and PCASP size distributions for the plumes are shown in Figure 10c and listed in Table 3. As noted in section 2.6, the PCASP measured heated, and therefore dry, aerosol. For the calculations of r_{eff} PCASP size distributions were modified to account for the effects of RH on particle size using the following equation [Hanel, 1976; Remer *et al.*, 1997]

$$r(RH) = r(RH_0) \left(\frac{100 - RH}{100 - RH_0} \right)^{-\gamma'} \quad (9)$$

where $r(RH)$ is the particle size at an ambient relative humidity and RH_0 is the dry relative humidity. The exponent γ' has values typically in the range of 0.1 to 0.3 [McMurry and Stolzenberg, 1989; Svenningsson *et al.*, 1992]. In this work we used a reference $RH_0 = 30\%$ and value of $\gamma' = 0.3$. Ferrare *et al.* [1998] found that a value of $\gamma' = 0.3$ provided the best match of optical properties calculated from PCASP measurements with Raman lidar profiles of extinction

and extinction/backscattering over the SGP site. This correction made about a 20% increase to the r_{eff} for the plumes with the highest RH.

Damoah et al. [2004] and Jaffe et al. [2004] have identified the presence of smoke plumes that originated in Siberia on about 17 May, and were transported at high altitude (4 to 5 km), arriving over northern Oklahoma on 26-28 May. Based on the altitude at which the plumes were encountered and other similar characteristics, plumes 11, 14, 15, 16, and 17 in Table 3 are identified as plumes originating from Siberia. It is possible that plumes 6 and 7 also originated from Siberia, however, their σ_{ep} and ω , as determined from Cadenza measurements of scattering and extinction and from nephelometer scattering and PSAP absorption, are lower than the other group of plumes. These are characterized by relatively high values of σ_{ep} and ω indicating that the smoke was significantly processed during transport [Damoah et al., 2004; Jaffe et al., 2004]. The trajectories suggest that the plume may have interacted with clouds during transport. In a study of four years of surface aerosol measurements at the SGP site, Sheridan et al. [2001] noted that aged smoke from Mexican fires had values of ω higher than the local smoke values. Inferring from their Figure 2, $\omega \approx 0.92$ (at 550 nm) for smoke from the 1998 Mexican fires which is comparable with the Siberian smoke plumes sampled in the AIOP, $\omega \approx 0.925$ (at 675 nm). The aged Siberian plumes were characterized by high $\sigma_{ep} \approx 50 \text{ Mm}^{-1}$, $\omega \approx 0.927$ (the neph+PSAP ω was 0.933), $r_{eff} \approx 0.2 \text{ }\mu\text{m}$, $\gamma \approx 0.14$, and a large accumulation mode within the range $0.3 \text{ }\mu\text{m} < D_p < 1.1 \text{ }\mu\text{m}$.

Figure 11 contrasts the size distribution measured during two plume events with those measured during level leg segments prior to the plumes. Figure 11a examines the low altitude smoke plume event of May 7 (plume 0 in Table 3) Figure 11b examines the high altitude plume on May 27 (plume 12 in Table 3) that was identified as part of the Siberian smoke plume discussed above.

Both plots show an increase in the accumulation mode that is responsible for the increase in extinction observed in the plumes. The extinction efficiency is highest in the size range from about 0.5 μm to 1.5 μm (diameter) causing higher extinction values. The size distribution of the Siberian biomass plume shows a peak at about 0.32 μm in contrast to the peak at about 0.15 μm for the fresh May 7th plume. This likely resulted from the growth of the Siberian smoke particles as they aged and were processed by clouds on their ten day transit from Siberia to Oklahoma. The ω values observed during these plume events also suggest that the Siberian plume consisted of aged aerosol.

The three grass fire plumes, plumes 0, 1, and 2, had relatively high r_{eff} , σ_{ep} , and relatively high ω . R_{eff} was highest for plumes 3 and 13. The size distribution for both of these plumes showed significant supermicron modes not observed in the other size distributions. Plume 3 was a low altitude plume with high extinction (164 Mm^{-1}). Plume 13 is characterized by a low altitude (2.56 km), high γ (0.38), and high r_{eff} (5.4). Therefore it is likely not associated with the Siberian event.

3.5 The Wavelength Dependence of Scattering Coefficient

The mission averaged Ångström exponents were 1.49 and 1.55 derived for the 467 nm to 530 nm wavelengths and 660 nm to 530 nm wavelength nephelometer scattering channels respectively. (Recall that the nephelometer scattering is reported at the PSAP wavelengths for this mission.)

The mission averaged Ångström exponent derived from the 1550 nm to 675 nm Cadenza extinction measurements was 1.64. These values suggest a slight non-linear character as is expected. To illustrate, scattering measurements averaged over the entire mission from the nephelometer and Cadenza are shown in Figure 12a as the natural log of the scattering

normalized to the 530 nm value versus the natural log of the wavelength. This plot shows scattering decreasing with an approximately linear dependence of -1.5 in agreement with the average Ångström exponents. Figure 12b shows that the wavelength dependence of scattering, averaged over only the plume cases, has increased only slightly to -1.4. This wavelength dependence is influenced by the inlet cut point, however, as illustrated in Table 3. For the column headed r_{eff} Equation 8 is integrated over the entire size distribution while for the column headed $r_{eff} < 2.7 \mu m$, Equation 8 is integrated only up to 2.7 μm Radius (5.4 μm diameter), simulating the r_{eff} of the aerosol measured in the by Cadenza, the nephelometer, and the PSAP. A comparison of the results shows that r_{eff} decreases dramatically for many of the plume cases due to inlet cutoff effects.

4. Conclusions

Cadenza is a new instrument which employs cavity ring-down to measure extinction coefficient and a reciprocal nephelometer technique to simultaneously measure scattering coefficient. The instrument measures extinction coefficient of 1 Mm^{-1} with an uncertainty of 2% at 675 nm wavelength; extinction coefficient of 5 Mm^{-1} with an uncertainty of 2% at 1550 nm wavelength; and scattering coefficient of 1 Mm^{-1} at 675 nm wavelength with an uncertainty of 10%. Instrument sensitivity is 0.3 Mm^{-1} in the visible and 0.5 Mm^{-1} in the infrared for a 8 second average.

Cadenza worked very well during the AIOP conducted in May of 2003. Continuous measurements of extinction and scattering were obtained for all flights. The instrument ran autonomously during the flights with no dropped data. Only minor adjustments to the cell alignment were performed between flights, although these were not strictly necessary to keep the

instrument running well. A mission-long comparison of 8 second averaged data showed excellent agreement between Cadenza extinction and the extinction coefficient formed by the sum of TSI nephelometer scattering plus PSAP absorption (Neph+PSAP). The comparison showed that, overall, Cadenza and the Neph+PSAP extinction coefficient values were within 2%, well within the measurement uncertainty of the Neph+PSAP. The overall comparison of Cadenza and TSI nephelometer scattering at 675 nm showed that Cadenza measured lower than the TSI nephelometer by about 2%, well within the uncertainty of the scattering measurement. Based on these correlations it we have demonstrated the ability to measure in-situ extinction and scattering to within several percent. The differences between Cadenza measurements and Neph+PSAP do not appear to be correlated with pressure, altitude, RH, or magnitude of extinction.

Comparisons between these instruments, made for the special case of plumes, showed that Cadenza measured extinction and scattering several percent higher on average than the Neph+PSAP and nephelometer alone. This difference is likely due to differences in the instrument response time: the response time for Cadenza is 1 sec while that for the nephelometer is a minimum of 8 sec.

The wavelength dependence of scattering, as determined from TSI nephelometer and Cadenza measurements, was nearly the same when averaged over the entire mission and over only the plumes cases. This similarity may be an artifact of the sampling characteristics of the aircraft inlet, however. The effective radius for the plume cases was calculated from size distributions composed of a composite of PCASP and CAPS measurements. The effective radius, when calculated between $0.11 < D_p < 5.5 \mu\text{m}$, was much smaller than that calculated over the entire size distribution. This was an indication of the effect of the aircraft inlet.

The aged plumes from Siberian forest fires were characterized by high altitudes (> 4 km), high $\sigma_{ep} \approx 50 \text{ Mm}^{-1}$, $\omega \approx 0.927$ (the neph+PSAP ω was 0.933), $r_{eff} \approx 0.2 \text{ }\mu\text{m}$, $\gamma \approx 0.14$, and a large accumulation mode within the range $0.3 \text{ }\mu\text{m} < D_p < 1.1 \text{ }\mu\text{m}$. In contrast, the fresh grass fire smoke was characterized by high instantaneous $\sigma_{ep} \approx 400\text{-}600 \text{ Mm}^{-1}$ (8-sec average $\approx 70 \text{ Mm}^{-1}$), $\omega \approx 0.918$, $r_{eff} \approx 1.31 \text{ }\mu\text{m}$, $\gamma \approx 0.17$, and a large particle mode with $D_p > 10 \text{ }\mu\text{m}$. Composite size distributions from wing-mounted probes showed that two of the plumes had significant large particle modes that resulted in high values of the effective radius. The effect of the large particle mode was not seen in the Ångström coefficient calculated from the in-cabin scattering measurements because of the characteristics of the aircraft inlet.

Cadenza has several advantages over other measurements of aerosol optical properties. In Cadenza both the scattering and the extinction of the aerosol are measured at the same time, under the same conditions and with the same temporal response. There is no instrumental temperature increase due to heat from the light source. In this study, the effect of relative humidity on scattering was measured at one wavelength with the humidified Radiance Research nephelometer, however, there is currently no instrument that can measure the effect of RH on absorption. Redemann et al. [2001] have estimated errors of as high as 0.03 in single-scattering albedo due to the assumption that the effect of relative humidity on the absorption coefficient is negligible. Coupling Cadenza with a humidification system would have the advantage that the effect of relative humidity for all of the optical properties, extinction, scattering, absorption, and single-scattering albedo can be obtained in one instrument at all of the measured wavelengths. The influence of relative humidity on absorption and single-scattering albedo is currently unknown and can be important for accurate climate modeling.

Acknowledgements: This work was made possible through the support of the DOE Atmospheric Radiation Measurement Program and the NASA Upper Atmospheric Research and Radiation Science Programs. One of the authors is supported by the National Research Council Associateship Program. We thank the CIRPAS pilots and support team for their hard work during the field missions.

5. References

- Anderson, T.L., D. Covert, et al., Performance characteristics of a high-sensitivity, three-wavelength, total scatter/backscatter nephelometer, *J. Atmos. and Oceanic Tech.*, 13 (5), 967, 1996.
- Anderson, T.L., and J.A. Ogren, Determining aerosol radiative properties using the TSI 3563 integrating nephelometer, *Aerosol Sci. Tech.*, 29, 57-69, 1998.
- Arnott, W.P., D. Covert, R. Elleman, J. Ogren, P.J. Sheridan, Rissman, and VanReken, Measurements of aerosol light absorption from meteorological aircraft using a photoacoustic instrument, this issue.
- Arnott, W.P., H. Moosmüller, P.J. Sheridan, J. Ogren, R. Raspert, W.V. Slaton, J.L. Hand, S.M. Kreidenweis, and J.L. Collett, Photoacoustic and filter-based ambient light absorption measurements: Instrument comparison and the role of relative humidity, *J. Geophys. Res.*, 108 (D1), 4034, 2003.
- Bane, J.M., R. Bluth, C. Flagg, J.H. H, W.K. Melville, M. Prince, and D. Riemer, UNOLS Overseas Research Aircraft Facilities for Ocean Science, *EOS Trans. AGU*, 85 (41), 402, 2004.
- Baumgardner, D., H. Jonsson, W. Dawson, and R. O'Commor Newton, The cloud, aerosol, and precipitation spectrometer: a new instrument for cloud investigations, *Atmos. Res.*, 59-60, 251-264, 2001.
- Bluth, R., P.A. Durkee, J.H. Seinfeld, R.C. Flagan, L.M. , P.A. Crowley, and P. Finn, Center for Interdisciplinary Remotely-Piloted Aircraft Studies (CIRPAS), *Bull. Am. Meteorol. Soc.*, 77, 2691-2699, 1996.
- Bond, T.C., T.L. Anderson, and D. Campbell, Calibration and intercomparison of filter-based measurement of visible light absorption by aerosols, *Aerosol Sci. Tech.*, 30, 582-600, 1999.
- Busch, K.W., and M.A. Busch, *Cavity Ringdown Spectroscopy*, American Chemical Society, Washington, D.C., 1999.
- Chylek, P., and J.A. Coakley, Aerosols and Climate, *Science*, 183, 75-77, 1974.
- Clarke, A.D., K.J. Noone, J. Heintzenberg, S.G. Warren, and D. Covert, Aerosol light absorption measurement techniques: Analysis and intercomparisons, *Atmos. Environ.*, 21, 1455-1465, 1987.
- Damoah, R., N. Spichtinger, C. Forster, P. James, I. Mattis, U. Wandinger, S. Beirle, T. Wagner, and A. Stohl, Around the world in 17 days - hemispheric-scale transport of forest fire smoke from Russia in May 2003, *Atmos. Chem. and Physics*, 4, 1311-1321, 2004.
- Dubovik, O., A. Smirnov, B.N. Holben, M.D. King, Y. Kaufman, T.F. Eck, and I. Slutsker, Accuracy assessment of aerosol optical properties retrieved from AERONET Sun and sky radiance measurements, *J. Geophys. Res.*, 105 (8), 9791-9806, 2000.
- Eck, T.F., B.N. Holben, et al., Variability of biomass burning aerosol optical characteristics in southern Africa during the SAFARI 2000 dry season campaign and a comparison of single scattering albedo estimates from radiometric measurements, *J. Geophys. Res.*, 108 (D13), 8477, doi:10.1029/2002JD002321), 2003.
- Ferrare, R., S.H. Melfi, D.N. Whiteman, K.D. Evans, M.R. Poellot, and Y.J. Kaufman, Raman lidar measurements of aerosol extinction and backscattering 2. Derivation of aerosol real refractive index, single-scattering albedo, and humidification factor using Raman lidar

- and aircraft size distribution measurements, *J. Geophys. Res.*, *103* (D16), 19673-19689, 1998.
- Ferrare, R., D. Turner, et al., Evaluation of Daytime Measurements of Aerosols and Water Vapor made by an Operational Raman Lidar over the Southern Great Plains, this issue.
- Fromm, M., R.M. Bevilacqua, J. Hornstein, E. Shettle, K.W. Hoppel, and J. Lumpe, An analysis of Polar Ozone and Aerosol Measurement (POAM) II Arctic polar stratospheric cloud observations, 1993-1996, *J. Geophys. Res.*, *104* (D20), 24341-24357, 1999.
- Gassó, S., D.A. Hegg, et al., Influence of humidity on the aerosol scattering coefficient and its effect on the upwelling radiance during ACE-2, *Tellus*, *52B*, 546-567, 2000.
- Gerber, H.E., Absorption of 632.8 nm radiation by maritime aerosols near Europe, *J. Atmos. Sci.*, *36*, 2502-2512, 1979a.
- Gerber, H.E., Portable cell for simultaneously measuring the coefficients of light scattering and extinction for ambient aerosols, *Applied Optics*, *18* (7), 1009-1014, 1979b.
- Hanel, G., An attempt to interpret the humidity dependencies of the aerosol extinction and scattering coefficients, *Atmos. Environ.*, *15*, 403-406, 1976.
- Hansen, J., M. Sato, A. Lacis, R. Ruedy, I. Tegen, and E. Matthews, Climate forcing in the industrial age, *Proc. Natl. Acad. Sci.*, *95*, 12753-12758, 1998.
- Hansen, J.E., and L.D. Travis, Light scattering in planetary atmospheres, *Space Sci. Rev.*, *16*, 527-610, 1974.
- Hegg, D.A., D.S. Covert, H. Jonsson, and P.A. Covert, Determination of the transmission efficiency of an aircraft aerosol inlet, *Aerosol Sci. and Tech.*, accepted.
- Heintzenberg, J., R.J. Charlson, A.D. Clarke, C. Liousse, V. Ramaswamy, K.P. Shine, M. Wendish, and G. Helas, Measurements and modeling of aerosol single-scattering albedo: progress, problems and prospects, *Beitr. Phys. Atmosph.*, *70* (4), 249-263, 1997.
- Horvath, H., Atmospheric light absorption - A review, *Atmos. Environ.*, *27A* (3), 293, 1993.
- Horvath, H., Experimental calibration for light absorption measurements using the integrating plate method, *J Atmos Sci*, *28*, 1149-1161, 1997.
- Houghton, J.T., Y. Ding, D.J. Griggs, M. Noguera, P.J.v.d. Linden, and S. Xiaosu, Climate change 2001: The Scientific Basis, Cambridge University Press, Cambridge, 2001.
- Jaffe, D., L. Bertshi, P. Jaegle, P. Novelli, J.S. Reid, H. Tanimoto, R. Vingarzan, and D.L. Westphal, Long-range transport of Siberian biomass burning emissions and impact on surface ozone in western North America, *Geophys. Res. Lett.*, *31* (doi: 10.1029/2004GL020093), 2004.
- Kasten, F., Visibility forecast in the phase of pre- condensation (Precondensation visibility dependence on aerosol particle swelling due to increasing humidity), *Tellus*, *21* (5), 631-635, 1969.
- Kiehl, J.T., and B.P. Briegleb, The relative roles of sulfate aerosols and greenhouse gases in climate forcing, *Science*, *260*, 311-314, 1993.
- McMurry, P.H., and M.R. Stolzenberg, On the sensitivity of particle size to relative humidity for Los Angeles aerosols, *Atmos. Environ.*, *23*, 497-507, 1989.
- Mitchell, D.L., Effective diameter in radiation transfer: General definition, applications, and limitations, *J Atmos Sci*, *59*, 2330-2346, 2002.
- Moosmüller, H., R. Varma, and W.P. Arnott, Cavity Ring-down and Cavity-Enhanced Detection Techniques for the Measurement of Aerosol Extinction, *Aerosol Sci. Tech.*, *39* (1), 30-39, 2005.

- Mulholland, G.W., and N.P. Bryner, Radiometric model of the transmission cell-reciprocal nephelometer, *Atmos. Environ.*, 28 (5), 873-887, 1994.
- O'Keefe, A., and D.A.G. Deacon, Cavity ring-down optical spectrometer for absorption measurements using pulsed laser sources, *Rev. Sci. Inst.*, 59 (12), 2544, 1988.
- O'Keefe, A., J.J. Scherer, and J.B. Paul, CW Integrated cavity output spectroscopy, *Chem. Phys. Lett.*, 307, 343-349, 1999.
- Paldus, B.A., and R.N. Zare, Absorption Spectroscopy: From early beginnings to cavity-ringdown spectroscopy, in *Cavity Ringdown Spectroscopy*, edited by K.W. Busch, and M.A. Busch, American Chemical Society, Washington, D.C., 1999.
- Pettersson, A., E.R. Lovejoy, C.A. Brock, S.S. Brown, and A.R. Ravishankara, Measurement of aerosol optical extinction at 532 nm with pulsed cavity ring-down spectroscopy, *J. Aerosol Sci.*, 35 (8), 995-1011, 2004.
- Press, W.H., B.P. Flannery, S.A. Teukolsky, and W.T. Vetterling, *Numerical Recipes*, 818 pp., University of Cambridge, 1986.
- Ramanathan, V., P.J. Crutzen, J.T. Kiehl, and D. Rosenfeld, Aerosol, climate and the hydrological cycle, *Science*, 294, 2119-2124, 2001.
- Ramanathan, V., P.J. Crutzen, A.P. Mitra, and D. Sikka, The Indian Ocean Experiment (INDOEX) and the Asian Brown Cloud, *Current Science*, 83 (8), 947-955, 2002.
- Redemann, J., P.B. Russell, and P. Hamill, Dependence of aerosol light absorption and single-scattering albedo on ambient relative humidity for sulfate aerosols with black carbon cores, *J. Geophys. Res.*, 106 (27), 27485-27495, 2001.
- Reid, J.S., P.V. Hobbs, C. Lioussé, J.V. Martins, R.E. Weiss, and T.F. Eck, Comparison of techniques for measuring shortwave absorption and black carbon content of aerosols from biomass burning in Brazil, *J. Geophys. Res.*, 103 (24), 332031, 1998.
- Remer, L.A., S. Gasso, D.A. Hegg, Y. Kaufman, and B.N. Holben, Urban/industrial aerosol: Ground-based Sun/sky radiometer and airborne in situ measurements, *J. Geophys. Res.*, 102 (16849-16859), 1997.
- Romanini, D., A.A. Kachanov, N. Sadeghi, and F. Stoeckel, CW cavity ring down spectroscopy, *Chem. Phys. Lett.*, 264 (3-4), 316-322, 1997.
- Russell, P.B., J. Redemann, et al., Comparison of aerosol single scattering albedos derived by diverse techniques in two North Atlantic experiments, *J. Atmos. Sci.*, 2001.
- Sappey, A.D., E.S. Hill, T. Settersten, and M.A. Linne, Fixed-frequency cavity ringdown diagnostic for atmospheric particulate matter, *Optics Letters*, 23 (12), 954-956, 1998.
- Schmid, B., R. Ferrare, et al., How well do state-of-the-art techniques measuring the vertical profile of tropospheric aerosol extinction compare?, this issue.
- Seinfeld, J.H., Scientific objectives, measurement needs, and challenges motivating the PARAGON aerosol initiative, *Bull. Am. Meteorol. Soc.*, 85 (10), 1503-1510, 2004.
- Seinfeld, J.H., and S.N. Pandis, *Atmospheric Chemistry and Physics: From Air Pollution to Climate Change*, John Wiley & Sons, Inc., New York, 1998.
- Sheridan, P.J., D.J. Delene, and J.A. Ogren, Four years of continuous surface aerosol measurements for the Department of Energy's Atmospheric Radiation Measurement Program Southern Great Plains Cloud and Radiation Testbed Site, *J. Geophys. Res.*, 106 (D18), 20735-20747, 2001.
- Siegman, A.E., *Lasers*, 1283 pp., University Science Books, Mill Valley, CA, 1986.

- Smith, J.D., and D.B. Atkinson, A portable pulsed cavity ring-down transmissometer for measurement of the optical extinction of the atmospheric aerosol, *Analyst*, 1126, 1216-1220, 2001.
- Strawa, A.W., R. Castaneda, T. Owano, D.S. Baer, and B.A. Paldus, The measurement of aerosol optical properties using continuous wave cavity ring-down techniques, *J. Atmos. Oceanic Tech.*, 20 (April), 454-465, 2003.
- Svenningsson, I.B., H.C. Hansson, and A. Weidenohler, Hygroscopic growth of aerosol particles in the Po Valley, *Tellus, Ser. B*, 42, 556-569, 1992.
- Van der Wal, R.L., and T.M. Ticich, Cavity ringdown and laser-induced incandescence measurements of soot, *Applied Optics*, 38 (9), 1444-1451, 1999.
- Virkkula, A., N.C. Ahlquist, D.S. Covert, W.P. Arnott, P.J. Sheridan, P.K. Quinn, and D.J. Coffman, Modification, calibration and a field test of an instrument for measuring light absorption by particles, *Aerosol Sci. Tech.*, 39 (1), 68-80, 2005.
- Weiss, R.E., and P.V. Hobbs, Optical extinction properties of smoke from the Kuwait oil fires, *J. Geophys. Res.*, 97, 14537-14540, 1992.
- Wexler, A.S., and J.H. Seinfeld, The distribution of ammonium salts among a size and composition dispersed aerosol, *Atmos. Environ.*, 24A, 1231-1246, 1990.

Table 1. Comparison of slope and correlation for Cadenza, Neph, and PSAP (8-sec avg.)			
	Slope	Y Intercept [Mm ⁻¹]	r ² correlation coefficient
Extinction, all flights	1.02	-0.81	0.978
Scattering, all flights	0.98	1.21	0.972
Extinction, last three flights	0.98	0.59	0.96
Scattering, last three flights	1.00	-0.59	0.954
Extinction, all profiles	0.99	0.41	0.986
Scattering, all profiles	0.96	1.96	0.982
Extinction, all plumes	1.097	-6.27	0.949
Scattering, all plumes	1.082	-5.22	0.956

Table 2. Profiles used in the analysis.				
Number	Date	Julian Date	Start Time	End Time
1	20030507	127	127.664	127.673
2	20030509	129	129.652	129.678
3	20030509	129	129.685	129.711
4	20030512	132	132.631	132.654
5	20030514	134	134.8	134.822
6	20030514	134	134.822	134.846
7	20030517	137	137.8	137.819
8	20030517	137	137.822	137.854
9	20030517	137	137.861	137.877
10	20030517	137	137.877	137.953
11	20030518	138	138.634	138.66
12	20030521	141	141.668	141.693
13	20030521	141	141.7	141.736
14	20030522	142	142.567	142.592
15	20030522	142	142.595	142.619
16	20030522	142	142.622	142.638
17	20030522	142	142.71	142.715
18	20030522	142	142.718	142.744
19	20030522	142	142.744	142.759
20	20030525	145	145.871	145.89
21	20030527	147	147.648	147.675
22	20030527	147	147.693	147.758
23	20030527	147	147.773	147.786
24	20030528	148	148.825	148.841
25	20030529	149	149.68	149.704

Table 3. Plumes used in the analysis										
#	Date	Start Time	End Time	Altitude	RH	Ext	SSA	r_{eff}	$r_{eff} < 2.7 \mu\text{m}$	gamma
—	—	Julian day	Julian day	Km	%	Mm^{-1}	—	μm	μm	—
0	20030507	127.742	127.743	0.787	60.6	62.97	0.927	1.71	0.215	0.167
1	20030507	127.801	127.801	0.411	49.3	64.36	0.923	1.12	0.195	-
2	20030507	127.804	127.805	0.412	48.8	71.22	0.906	0.914	0.197	-
3	20030515	135.691	135.704	0.698	88.6	163.6	0.958	7.32	0.743	0.466
4	20030522	142.613	142.626	0.887	40.2	40.97	0.912	—	—	0.3527
5	20030527	147.614	147.62	2.84	10.8	52.46	0.949	0.351	0.243	0.172
6	20030527	147.626	147.629	5.18	6.97	22.11	0.861	0.262	0.221	0.127
7	20030527	147.649	147.651	5.13	3.86	23.39	0.871	0.204	0.192	—
8	20030527	147.655	147.665	3.22	8.49	66.96	0.946	0.25	0.229	—
9	20030527	147.707	147.723	2.37	18.5	64.67	0.943	0.261	0.223	0.144
10	20030527	147.724	147.731	3.33	5.92	100.3	0.965	0.262	0.237	0.109
11	20030527	147.75	147.756	4.77	4.81	57.72	0.932	0.21	0.201	0.144
12	20030527	147.775	147.781	3.69	5.31	52.1	0.864	0.225	0.215	0.171
13	20030528	148.813	148.818	2.56	87.9	66.48	0.961	5.4	0.985	0.38
14	20030528	148.834	148.837	4.09	24.8	39.08	0.9	0.205	0.186	0.118
15	20030528	148.855	148.867	4.15	7.53	49.09	0.936	0.192	0.185	0.122
16	20030528	148.87	148.874	4.33	6.85	52.61	0.94	0.191	0.188	0.108
17	20030528	148.878	148.882	4.43	5.32	72.42	0.962	0.192	0.186	0.141

Figure Captions

Figure 1. Schematic of the Cadenza Instrument - Flow and Optical Cell.

Figure 2. Smoke visualization of test cell showing the laminar flow boundary between the purge and aerosol sample flows.

Figure 3. Picture of Cadenza mounted in a 19-inch equipment rack in our lab showing overall height of 40 inches.

Figure 4. Calibration plots for Cadenza showing extinction or scattering calculated for PSL using the CPC number density versus measured extinction or scattering. a) 675 nm extinction, b) 675 nm scattering, c) 1550 nm extinction.

Figure 5a. Scatter plot of Cadenza and Neph Scattering coefficient. 20744 8-sec averages are corrected to ambient temperature, pressure, and relative humidity are plotted. (See text for details.) The nephelometer data is converted to 675 nm using the nephelometer-derived Ångström exponent.

Figure 5b. Scatter plot of Cadenza and Neph+PSAP Extinction coefficient. 20744 8-sec averages are corrected to ambient temperature, pressure, and relative humidity are plotted. (See text for

details.) The nephelometer data is converted to 675 nm using the nephelometer-derived Ångström exponent and the PSAP data is converted to 675 nm using a λ^{-1} correction.

Figure 6. Comparison of Extinction and scattering measurements made on May 7, 2003. a) Altitude profile for the day's flight. b) Comparison of Cadenza and Neph+PSAP extinction coefficient measurements at 675 nm. c) Comparison of Cadenza and nephelometer scattering coefficient measurements at 675 nm. d) Comparison of 1-sec scattering data for the three plumes indicated in Figure 6c to illustrate the effects of sampling time on the measurement of plumes. Note that the time is in fractional Julian days. The 1 second data in Figure 6d are not corrected for truncation error.

Figure 7. Comparison of aerosol optical properties for May 27, 2003. 8 sec. averages versus mission time in fractional Julian days. a) Cadenza and neph+PSAP extinction at 675 nm wavelength, b) Cadenza and nephelometer scattering at 675 nm wavelength, c) Cadenza extinction coefficient at 1550 nm wavelength, d) altitude and ambient relative humidity and temperature.

Figure 8. Comparison of Cadenza and AATS-14 extinction profiles for May 27, profile 22.

Figure 9. A comparison of four profiles illustrating the variability of aerosol extinction with altitude.

Figure 10. Measured a) extinction coefficient, b) single-scattering albedo, and c) effective radius calculated from the composite size distributions which were adjusted to ambient relative humidity averaged over the plumes listed in Table 3.

Figure 11. Composite size distributions of two types of plumes compared with non plume events. a) low altitude smoke plume event (plume 0) with that measured just prior to the event. b) high altitude plume on May 27 (plume 12), identified as originating in Siberia, and a level leg measured just prior to the event.

Figure 12. Wavelength dependence of scattering coefficient derived from the TSI nephelometer and Cadenza for the plumes designated in Table 3. a) mission average, b) plume average.

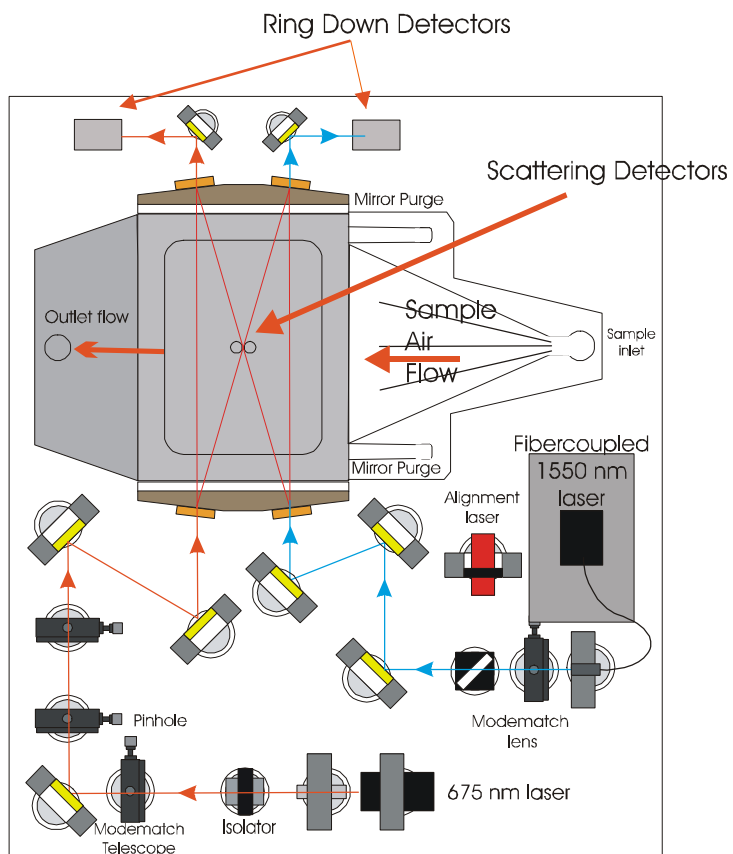


Figure 1. Schematic of the Cadenza Instrument - Flow and Optical Cell.

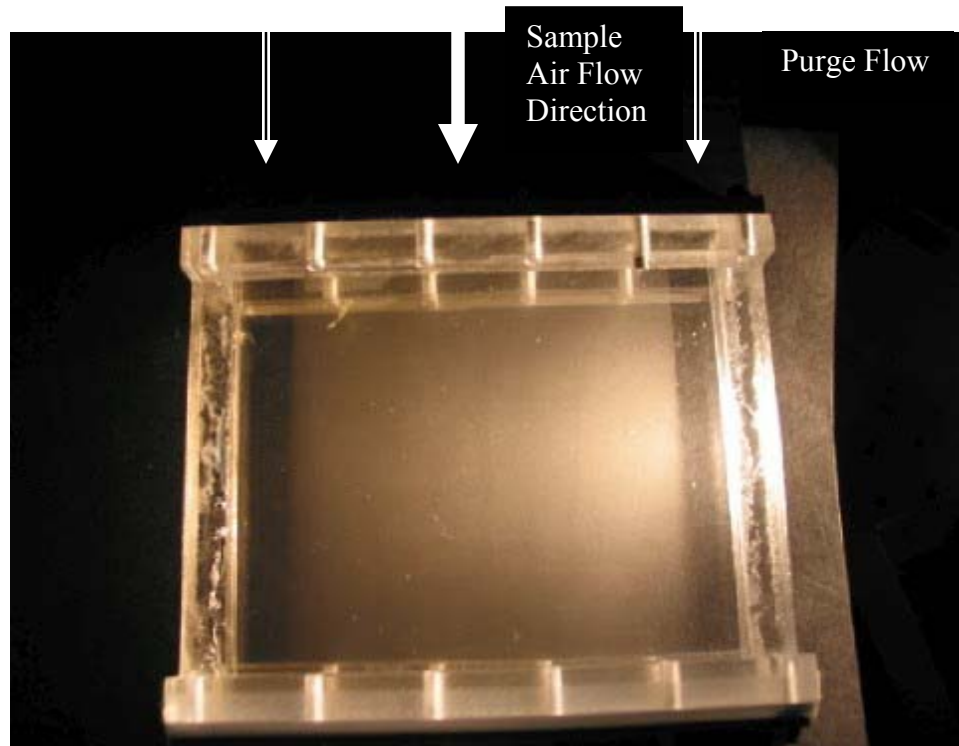


Figure 2. Smoke visualization of test cell showing the laminar flow boundary between the purge and aerosol sample flows.

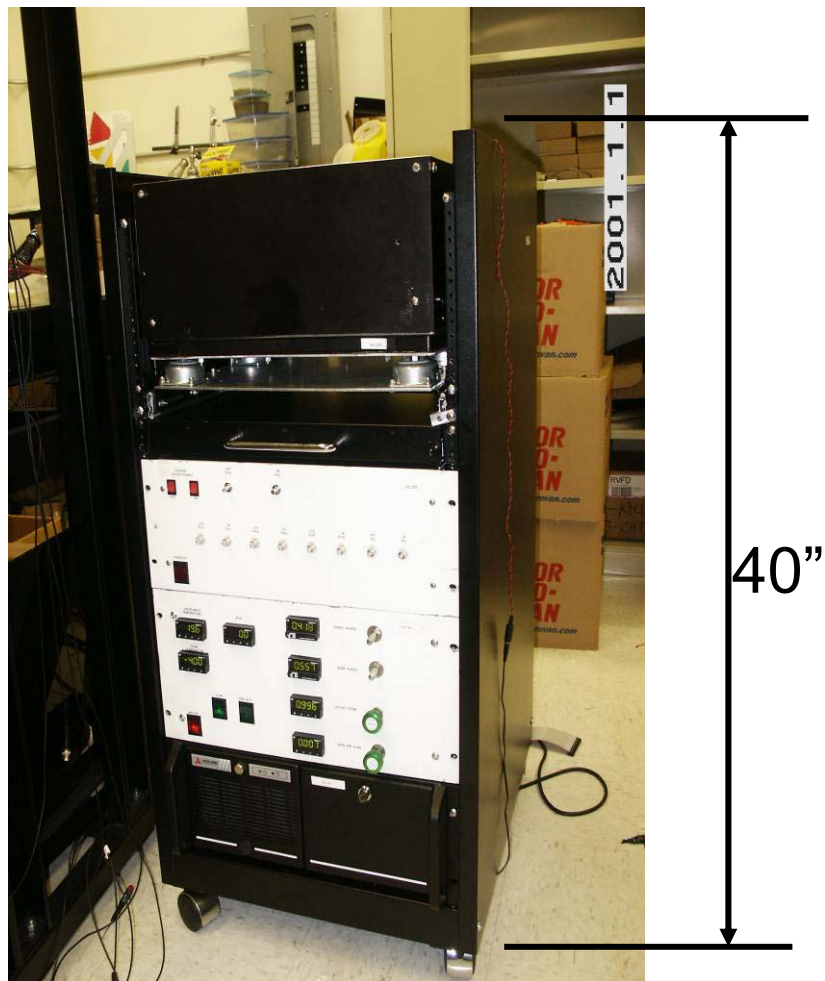


Figure 3 Picture of Cadenza mounted in a 19-inch equipment rack in our lab showing overall height of 40 inches.

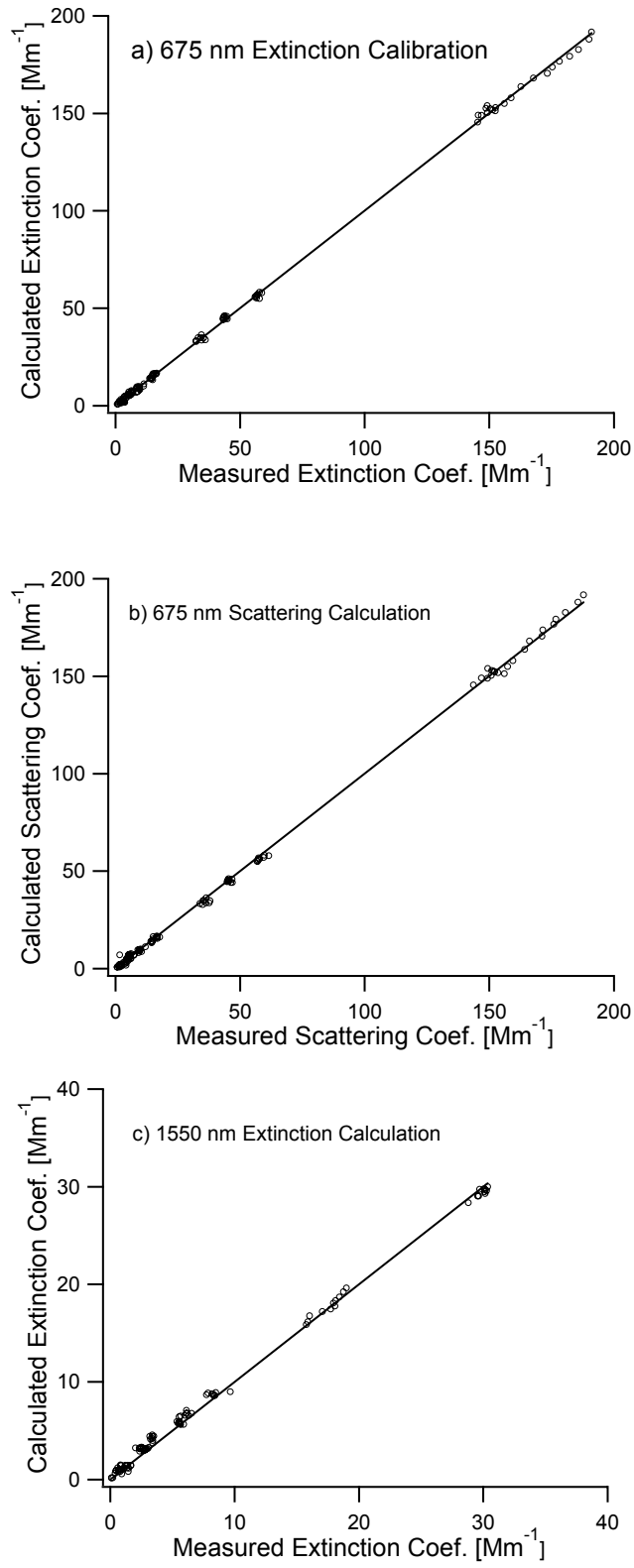


Figure 4

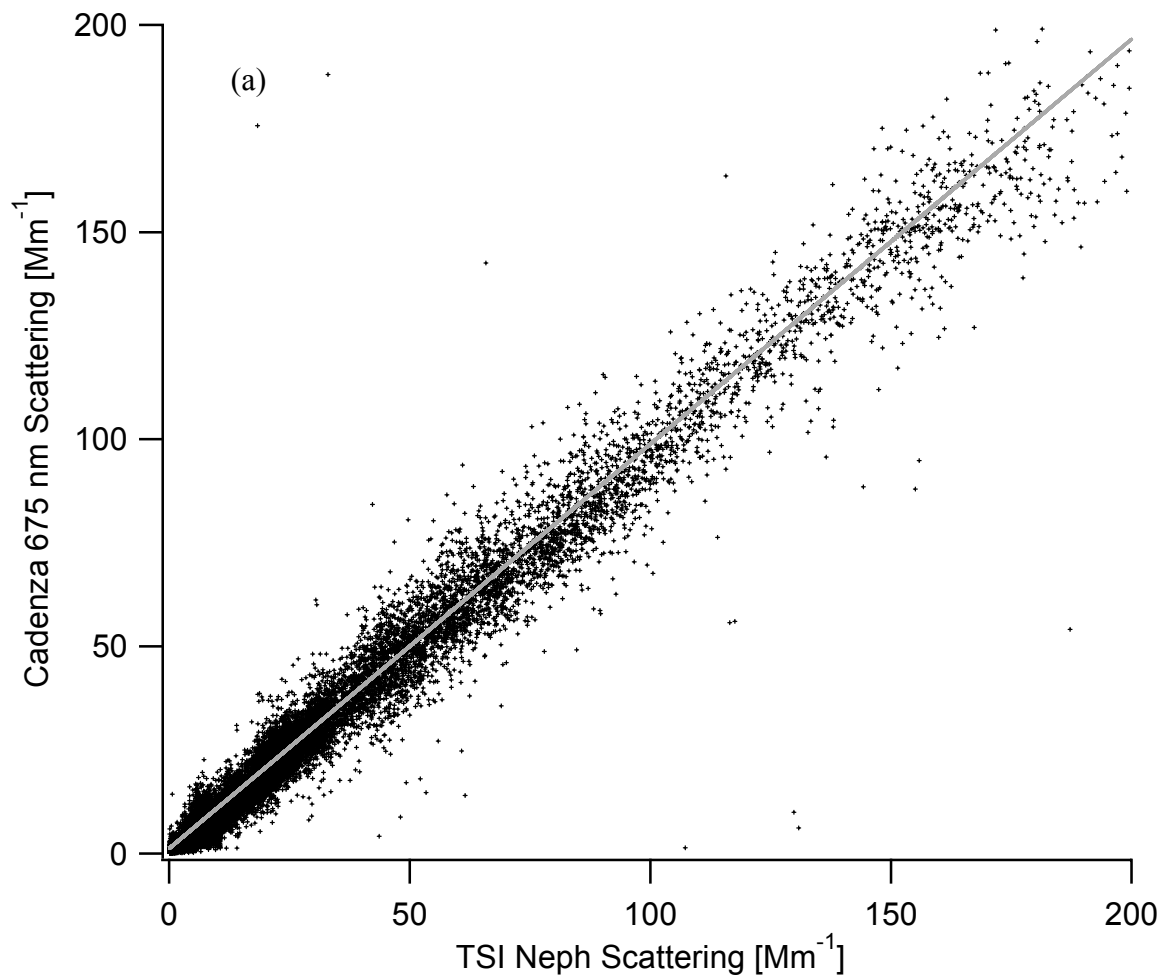


Figure 5a. Scatter plot of Cadenza and Neph Scattering coefficient. 20744 8-sec averages are corrected to ambient temperature, pressure, and relative humidity are plotted. (See text for details.) The nephelometer data is converted to 675 nm using the nephelometer-derived Ångström exponent.

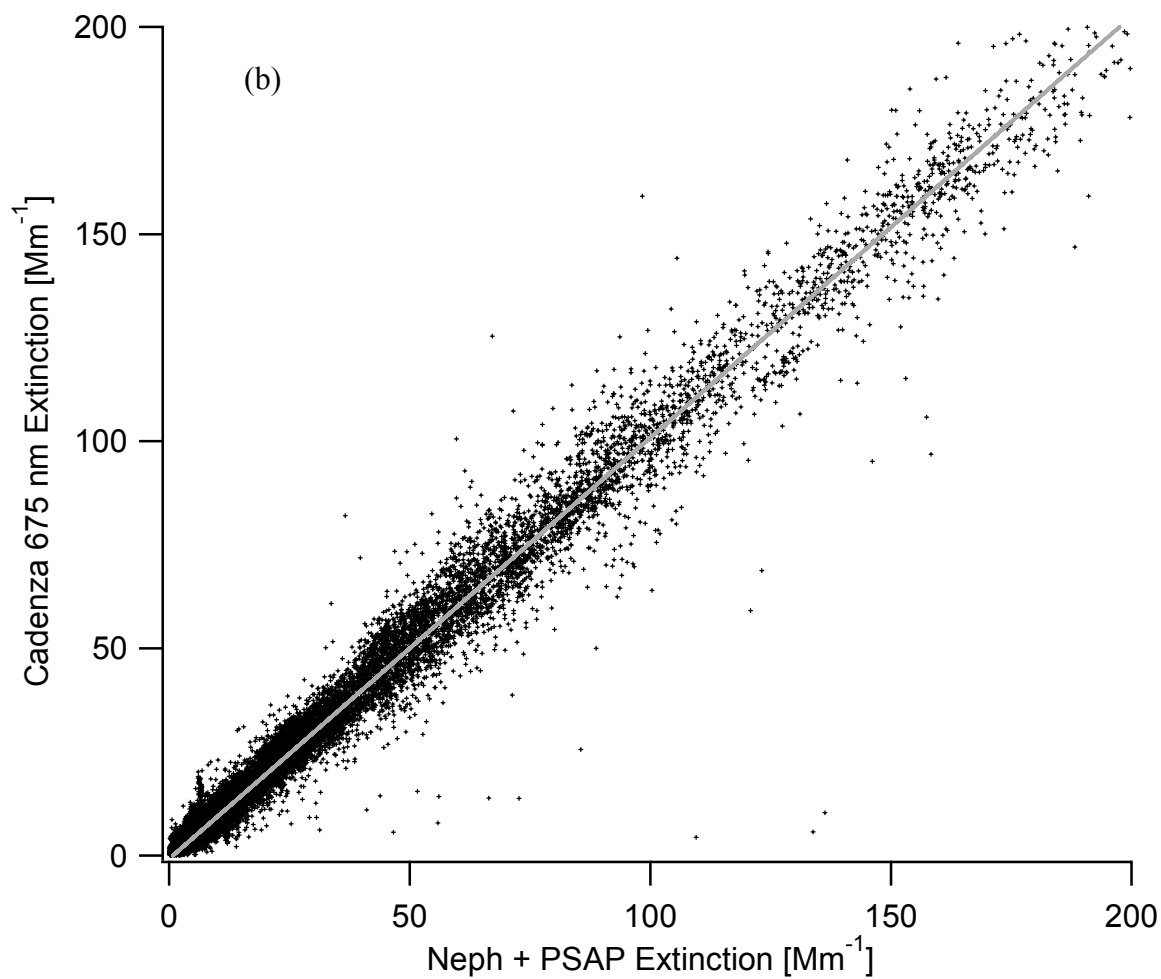


Figure 5b. Scatter plot of Cadenza and Neph+PSAP Extinction coefficient. 20744 8-sec averages are corrected to ambient temperature, pressure, and relative humidity are plotted. (See text for details.) The nephelometer data is converted to 675 nm using the nephelometer-derived Ångström exponent and the PSAP data is converted to 675 nm using a λ^{-1} correction.

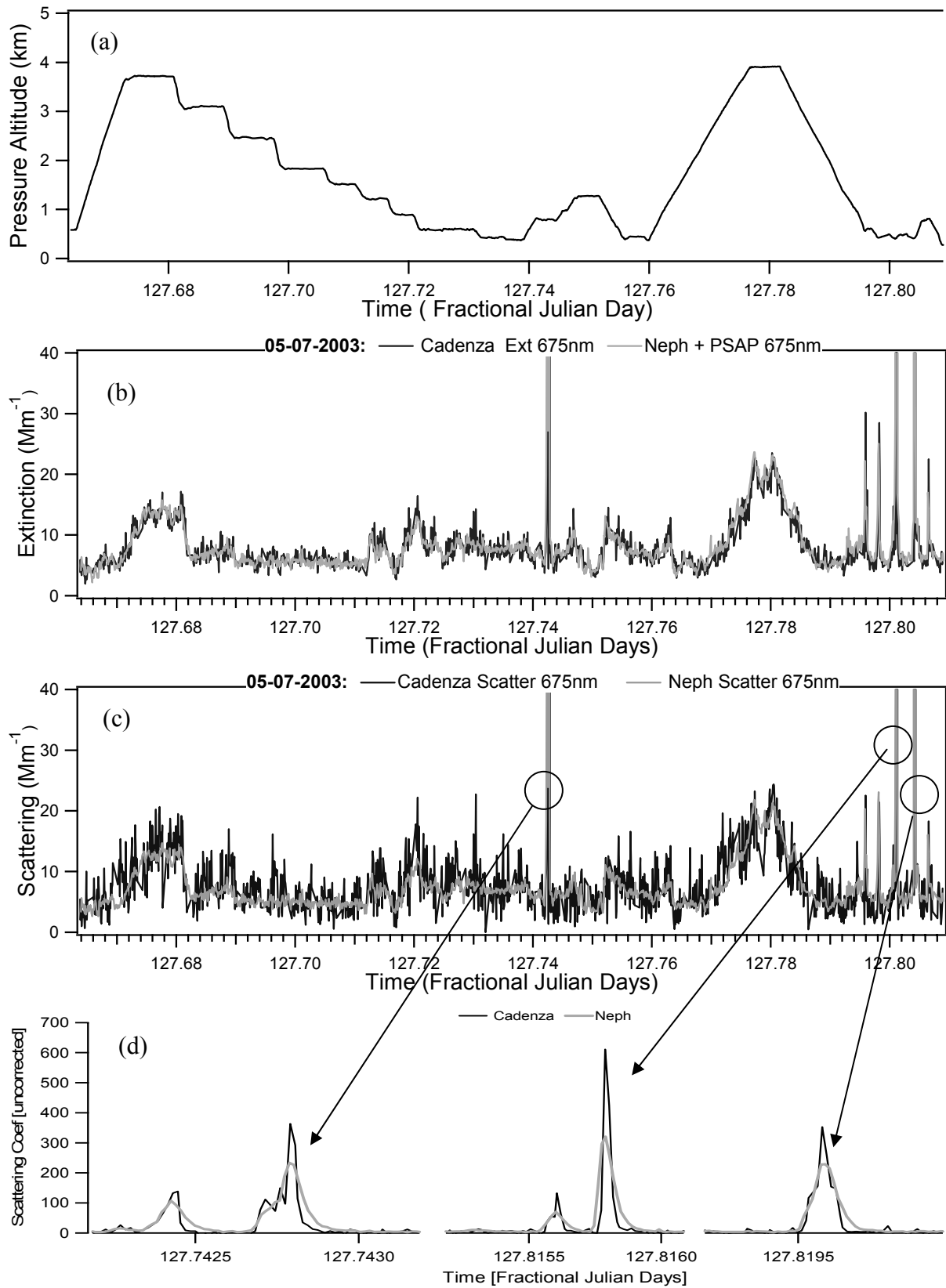


Figure 6

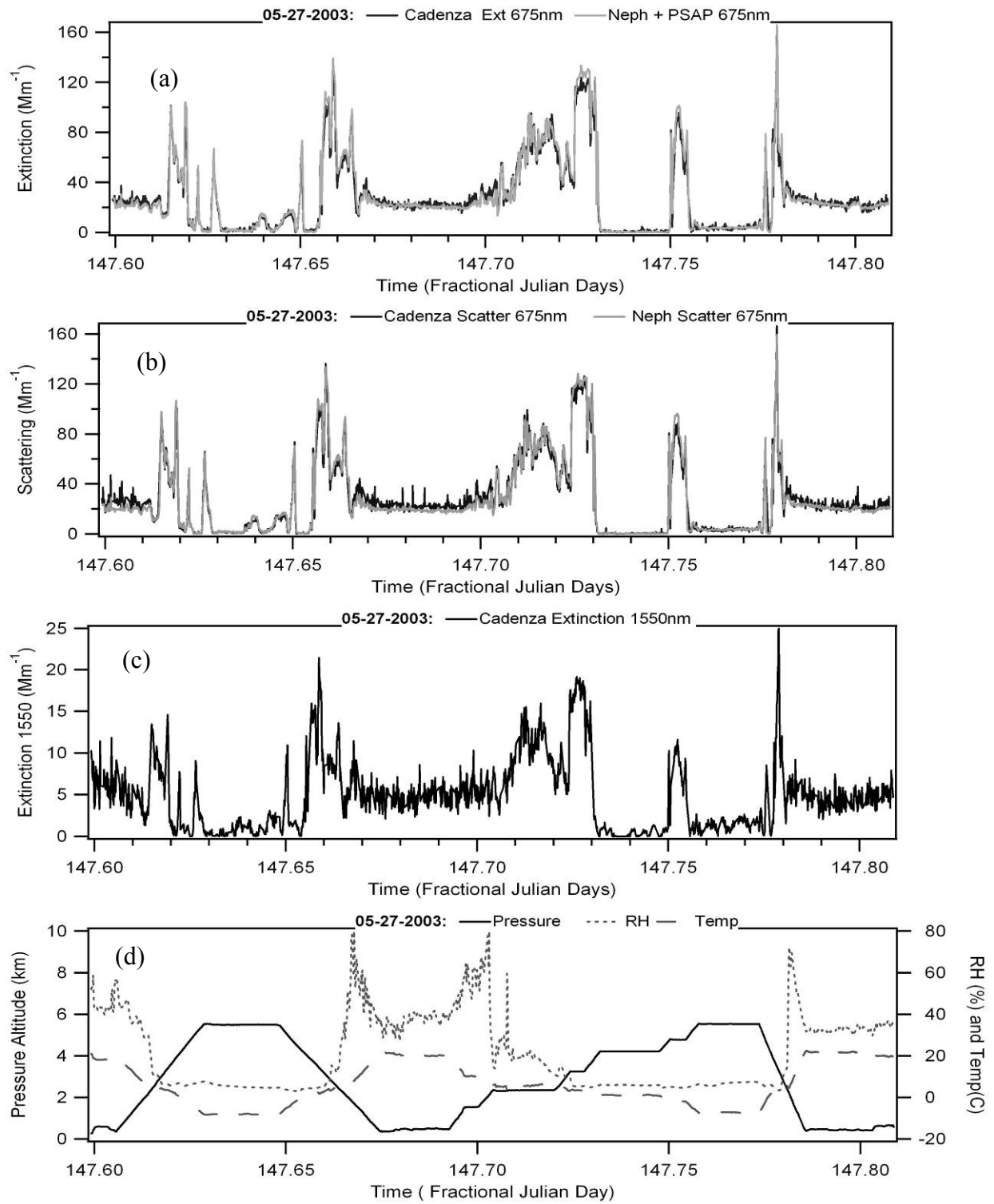


Figure 7.

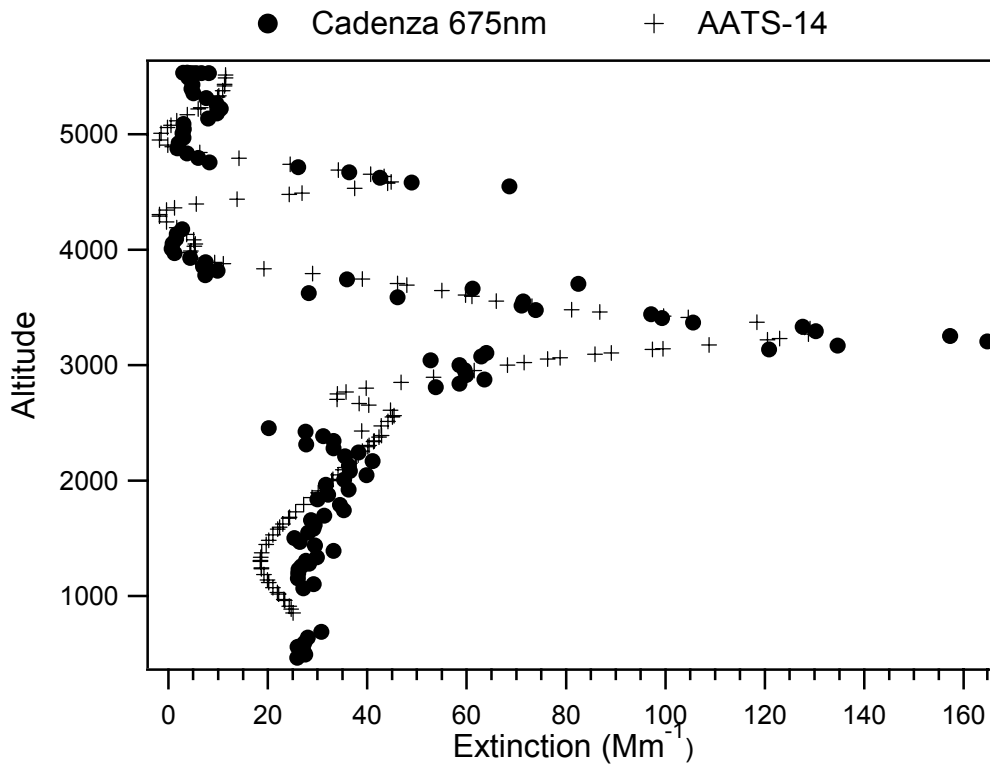


Figure 8. Comparison of Cadenza and AATS-14 extinction profiles for May 27, profile 22.

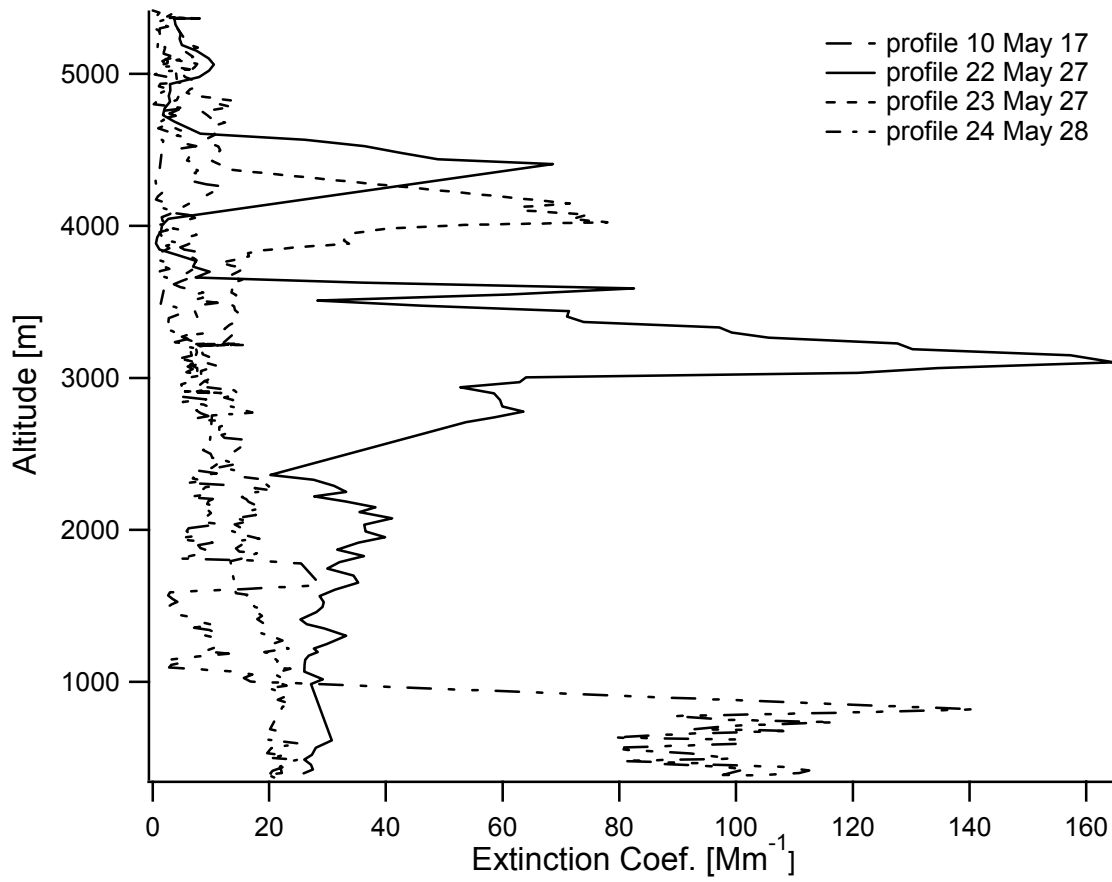


Figure 9. A comparison of four profiles illustrating the variability of aerosol extinction with altitude.

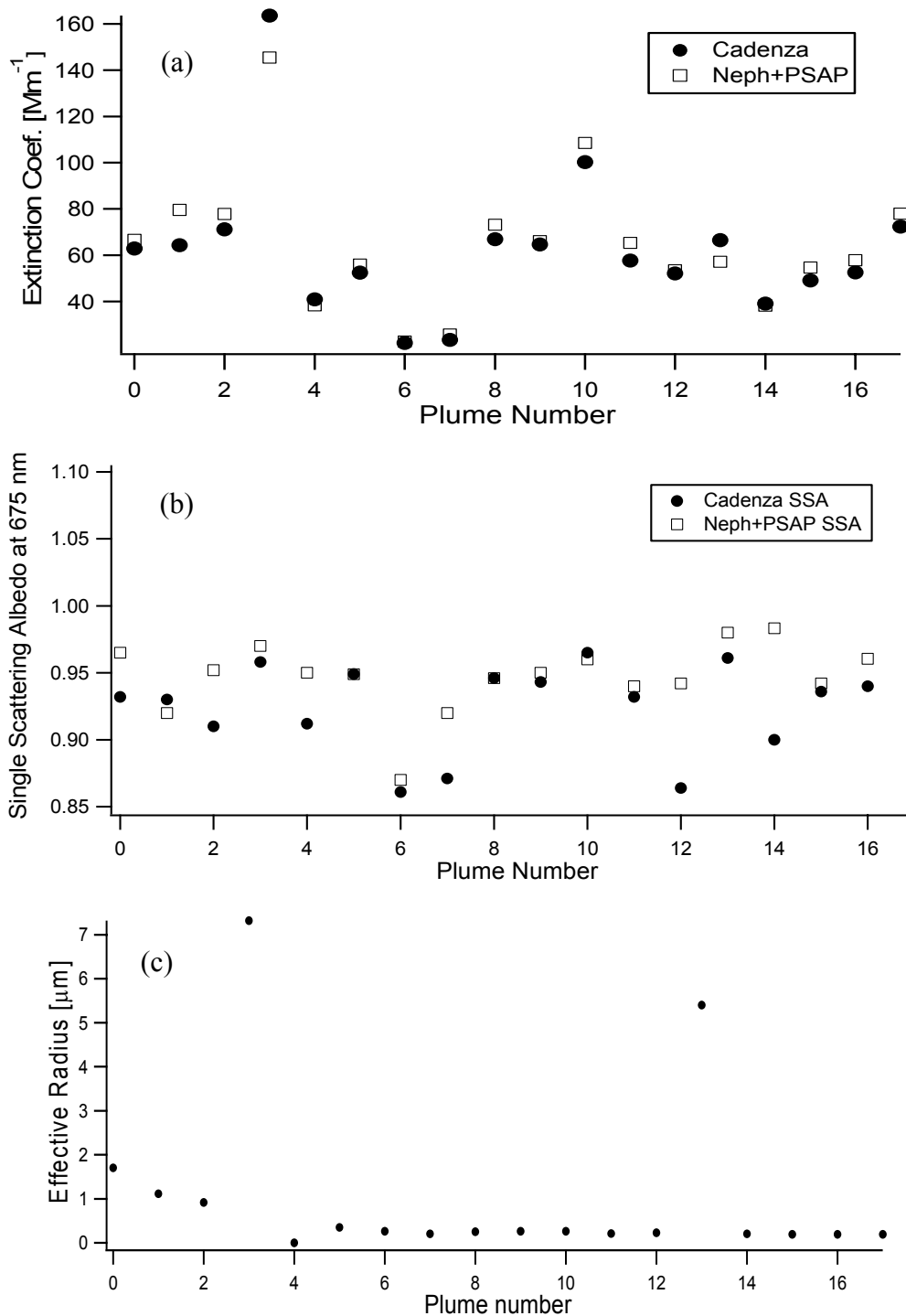


Figure 10. Measured a) extinction coefficient, b) single-scattering albedo, and c) effective radius calculated from the composite size distributions which were adjusted to ambient relative humidity averaged over the plumes listed in Table 3.

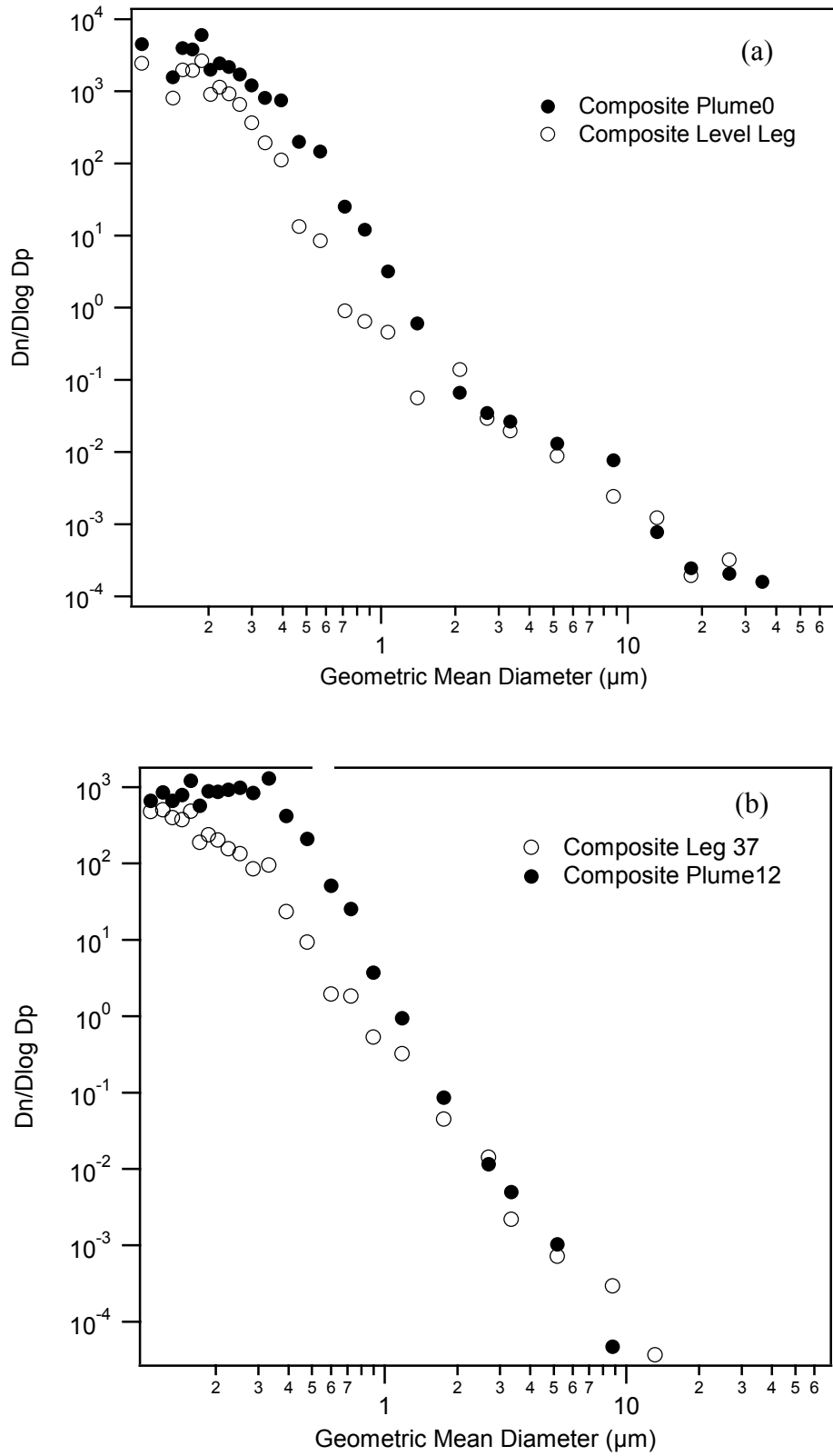


Figure 11.

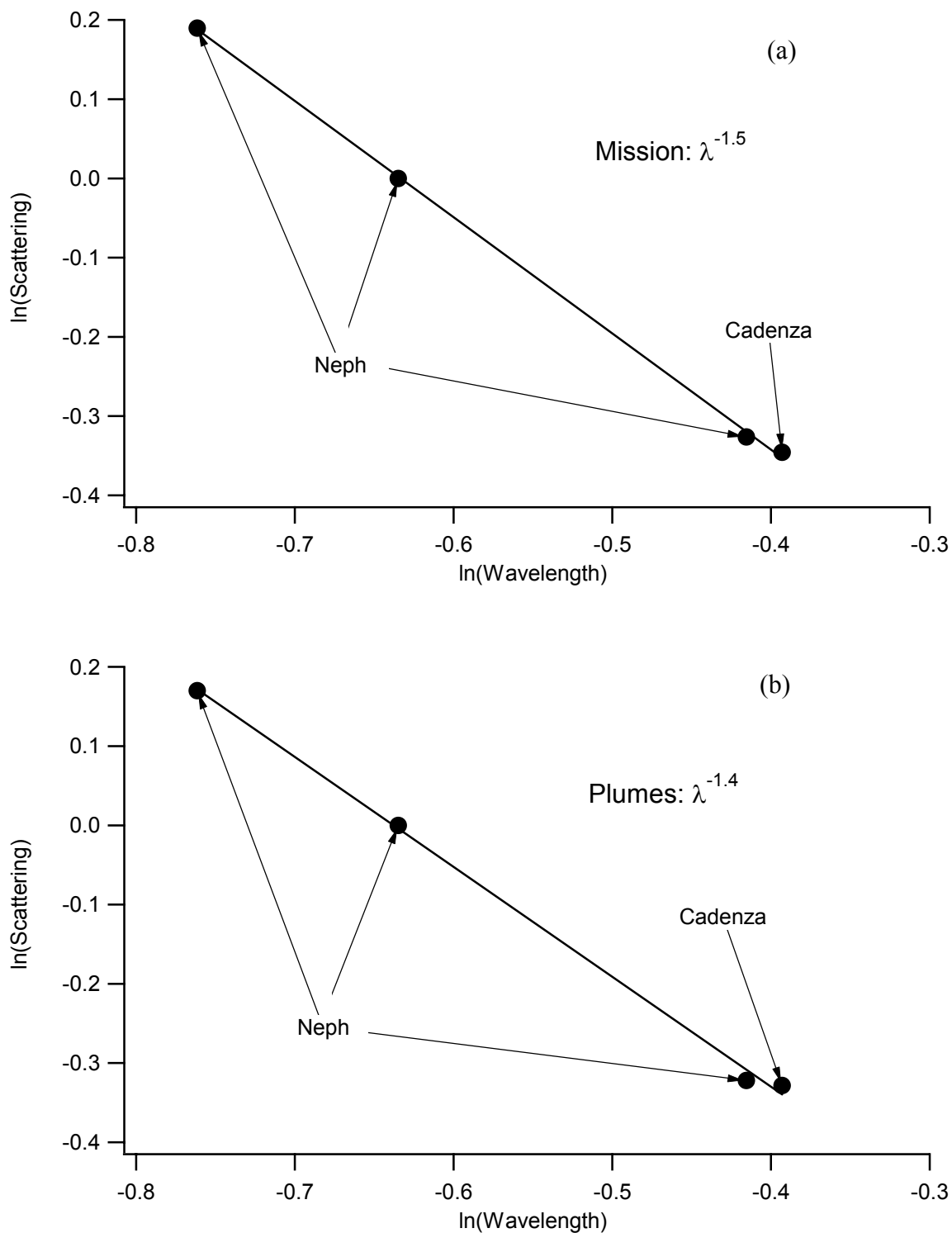


Figure 12. Wavelength dependence of scattering coefficient derived from the TSI nephelometer and Cadenza for the plumes designated in Table 3. a) mission average, b) plume average.